Regulatory T cells suppress the formation of super-effector CD8 T cells by limiting IL-2

Oksana Tsyklauri[1, 2], Tereza Chadimova[1,2], Veronika Niederlova[1], Jirina Kovarova[3], Juraj Michalik[1], Iva Malatova[3], Sarka Janusova[1], Helene Rossez[4], Ales Drobek[1], Hana Vecerova[1], Virginie Galati[4], Marek Kovar[3], Ondrej Stepanek[1,4*]

[1] Laboratory of Adaptive Immunity, Institute of Molecular Genetics of the Czech Academy of Sciences, Prague, Czech Republic

[2] Faculty of Science, Charles University, Prague, Czech Republic

[3] Institute of Microbiology of the Czech Academy of Sciences, Prague, Czech Republic

[4] Department of Biomedicine, University Hospital and University of Basel, Basel, Switzerland

[*]Correspondence should be addressed to Ondrej Stepanek:
ondrej.stepanek@img.cas.cz

Abstract

Regulatory T cells (Tregs) are indispensable for maintaining self-tolerance by suppressing conventional T cells. On the other hand, Tregs may promote tumor growth by inhibiting anti-cancer immunity. In this study, we identified that Tregs increase the quorum of self-reactive $CD8^+$ T cells required for the induction of experimental autoimmune diabetes. Their major suppression mechanism is limiting available IL-2, a key cytokine for activated T cells. Specifically, Tregs inhibit the formation of a previously uncharacterized subset of antigen-stimulated $CD8^+$ T cells. Since these T cells express high levels of IL-7 receptor and cytotoxic molecules (KLRK1, GZMB), and show superior cell killing abilities, we call them super-effector T cells. The administration of agonistic IL-2 immunocomplexes phenocopies the absence of Tregs, i.e., it induces super-effector T cells, promotes autoimmunity, and enhances anti-tumor responses. Counterparts of super-effector T cells were found in the human blood, revealing them as a potential target for immunotherapy.

Introduction

Physiological immune responses aim at invading pathogens, but not at healthy tissues. A failure of this self-tolerance principle leads to the development of autoimmune diseases, such as type I diabetes. On the other hand, the mechanisms of self-tolerance also inhibit anti-tumor immune responses. There are two major principles of controlling self-reactive lymphocytes: clonal deletion (central tolerance) and suppression (peripheral tolerance).

FOXP3$^+$ regulatory T cells (Tregs) represent a major force of peripheral tolerance as they regulate homeostasis and immune responses of conventional T cells [1]. The absence of Tregs in FOXP3-deficient individuals leads to a severe autoimmune condition called immunodysregulation polyendocrinopathy enteropathy X-linked syndrome [2-4]. Accordingly, Tregs inhibit anti-tumor immune responses.

Although most studies have focused on how Tregs suppress conventional CD4$^+$ T cells, CD8$^+$ T cells are regulated by Tregs as well. In the steady-state, Tregs suppress the proliferation of CD8$^+$ T cells [5] and prevent the spontaneous differentiation of memory CD8$^+$ T cells into effector cells [6, 7]. Moreover, Tregs suppress antigenic responses of CD8$^+$ T cells [8-10]. Multiple mechanisms of Treg-mediated suppression of CD8$^+$ T cells have been proposed, such as reducing the expression of co-stimulatory molecules on antigen-presenting cells (APC) via CTLA4 [7, 9, 11], limiting the availability of IL-2 [8, 9], production of anti-inflammatory cytokines IL-10 [6] and TGFβ [12], and limiting the production of CCL3, CCL4, and CCL5 chemokines by APCs [10].

A single study addressed how Tregs suppress CD8$^+$ T-cell responses with various affinity to the cognate antigen [11]. The authors concluded that Tregs inhibit CD8$^+$ T-cell activation by low-affinity, but not high-affinity, antigens. In such a case, Tregs would not correct errors of central tolerance by suppressing highly self-reactive CD8$^+$ T cells escaping negative selection in the thymus. Their tolerogenic role would be limited to increasing the antigen-affinity threshold in the periphery [13] by suppressing positively selected CD8$^+$ T cells with intermediate to low affinity to self-antigens.

In this study, we focused on Treg-mediated peripheral tolerance, which prevents self-reactive CD8$^+$ T cells from inducing an autoimmune pathology. We observed that Tregs increase the initial number of self-reactive CD8$^+$ T cells required for the induction of experimental diabetes across a wide range of their affinities to self-antigens. The major mechanism of Treg suppression is limiting the availability of IL-2, a cytokine triggering the formation of potent CD8$^+$ super-effector T cells in high concentrations. Accordingly, excessive IL-2 signal prevents Tregs from suppressing CD8$^+$ T cells in vitro as well as during autoimmune and anti-tumor responses in vivo.

Results

Tregs increase the quorum of self-reactive CD8$^+$ T cells for inducing an autoimmune pathology

To study the potential role of FOXP3$^+$ Tregs in the autoimmune response of self-reactive T cells, we employed a model of experimental autoimmune diabetes based on the transfer of ovalbumin (OVA)-specific OT-I T cells into double-transgenic mice expressing ovalbumin in pancreatic β-cells [14] and diphtheria toxin receptor (DTR) in FOXP3$^+$ Tregs. Most of the experiments were done with RIP.OVA DEREG mice carrying a random insertion of a transgene encoding for DTR-GFP fusion protein under the control of *Foxp3* promoter [15], but some experiments were performed also in *Foxp3^{DTR}* RIP.OVA strain with *DTR-GFP* knocked-in into the 3' untranslated region of the *Foxp3* locus [16]. Subsequent priming of OT-I T cells induced the formation of effector T cells and eventual destruction of pancreatic β-cells. The administration of diphtheria toxin (DT) selectively depleted Tregs uncovering their role in this autoimmune pathology. The major advantages of this model are: i) known etiology – the pathology is triggered by self-reactive CD8$^+$ T cells, ii) control of key parameters (number of transferred OT-I T cells, affinity of the priming antigen, Treg presence etc.), and iii) the by-pass of central tolerance enabling us to study mechanisms of peripheral tolerance separately from the central tolerance.

The induction of diabetes in the majority of Treg-replete mice required 10^6 adoptively transferred OT-I T cells followed by priming with OVA peptide and LPS (Fig. 1A-C). This revealed efficient mechanisms of peripheral tolerance preventing the self-reactive T cells from destroying insulin-producing cells. After the depletion of Tregs, the number of transferred OT-I T cells sufficient to induce diabetes in the vast majority of animals dropped by two orders of magnitude (Fig. 1B-C). Accordingly, the expansion of OT-I T cells was enhanced in Treg-deficient mice in comparison to Treg-replete mice (Fig. 1D, Fig. S1A-B). When 10^6 OT-I T cells were transferred, 50 % of Treg-depleted mice developed diabetes even when they were primed with LPS alone without the cognate peptide (Fig. 1E, Fig. S1C). This was possible because the small amount of endogenous OVA was sufficient to prime OT-I T cells, as revealed by comparing the expansion and CD44$^+$ CD62L$^-$ effector T-cell formation in RIP.OVA, *Foxp3^{DTR}* RIP.OVA, and *Foxp3^{DTR}* mice (Fig. 1F, Fig. S1D). Overall, these results revealed that Tregs represent a major mechanism of peripheral tolerance preventing diabetes induction by self-reactive CD8$^+$ T cells.

To study how Tregs suppress priming of self-reactive T cells by antigens with various affinities, we adopted a priming protocol based on the adoptive transfer of bone marrow-derived dendritic cells (DCs) loaded with OVA peptide (K_D ~ 50 μM) or its variants recognized by OT-I T cells with lower affinity; Q4R7 (K_D ~ 300 μM) or Q4H7 (K_D ~ 850 μM) [17]. In contrast to OVA peptide and LPS priming, as few as 10^3 transferred OT-I T cells were able to induce autoimmune diabetes in RIP.OVA mice upon DC-OVA priming (Fig. 2A).

When 3×10^2 OT-I T cells were transferred, all Treg-depleted mice, but only one third of Treg-replete mice, were diabetic (Fig. 2A). Accordingly, the absence of Tregs increased the susceptibility to diabetes upon priming with DC-Q4R7, although as many as 3×10^4 OT-I T cells were required to induce diabetes in most Treg-depleted hosts (Fig. 2B). Along this line, Treg-replete RIP.OVA mice were resistant to 10^6 OT-I T cells primed with DC-Q4H7, whereas most Treg-depleted mice manifested diabetes (Fig. 2C). The expansion of OT-I T cells, their expression of IL-2Rα (CD25; a subunit of high-affinity IL-2 receptor) and KLRG1 (a marker of short-lived effector cells), and the absolute count of KLRG1$^+$ OT-I T cells in the spleen were greater in Treg-depleted than in Treg-replete RIP.OVA mice on day six post-immunization with DC-OVA, -Q4R7, or -Q4H7 (Fig. 2D-F, S2A-C). DCs not loaded with any peptide did not induce diabetes with one exceptional mouse (Fig. S2D-E). Collectively, these results showed that Tregs increased the quorum of self-reactive CD8$^+$ T cells required for inducing autoimmune diabetes irrespective of the priming antigen affinity, while preserving the hierarchy of the biological potencies of these antigens (Fig. S2F).

To elucidate, whether the physiological activity of Tregs is a limiting factor of self-tolerance, we selectively expanded the Treg compartment prior to the diabetes induction using complexes of IL-2 and anti-IL-2 mAb JES6-1A12 (JES6) [18, 19] (Fig. 2G). We observed that the expanded Tregs prevented DC-OVA induced diabetes in most animals (Fig. 2H), showing that enhancing the overall Treg activity increases self-tolerance and prevents the induction of the experimental diabetes.

Tregs suppress self-reactive CD8$^+$ T cells in the absence of conventional CD4$^+$ T cells

Tregs could inhibit self-reactive CD8$^+$ T cells directly or via suppressing a by-stander help of CD4$^+$ T cells. To address this question, we used T-cell deficient *Cd3ε*$^{-/-}$ RIP.OVA mice as hosts. First, we adoptively transferred 10^6 polyclonal OVA-tolerant CD8$^+$ T cells isolated from RIP.OVA mice to replenish the CD8$^+$ T-cell compartment in the *Cd3ε*$^{-/-}$ RIP.OVA mice. A week later, we transferred conventional (*Foxp3-GFP*$^-$) or Treg (*Foxp3-GFP*$^+$) CD4$^+$ T cells from DEREG RIP.OVA mice. A control group of mice did not receive any CD4$^+$ T cells. Finally, we transferred OT-I T cells and subsequently primed them with DC-OVA (Fig. 3A). We observed that conventional CD4$^+$ T cells, albeit presumably tolerant to OVA, increased the incidence of experimental diabetes and accelerated its onset (Fig. 3B-C, S3A). In contrast, Tregs reduced the incidence of diabetes in comparison to mice receiving no CD4$^+$ T cells (Fig. 3B-C, S3A). Conventional CD4$^+$ T cells enhanced the expansion of OT-I T cells and increased the number of KLRG1$^+$ OT-I T cells, whereas Tregs elicited the opposite effect (Fig. 3D-E, Fig. S3B-C), as revealed on day eight post-immunization. The role of Tregs was even more apparent on day 14 post-immunization, which corresponded to the typical onset of diabetes in the absence of conventional CD4$^+$ T cells (Fig. 3F-G, Fig. S3D-E).

Overall, these experiments showed that conventional $CD4^+$ T cells provide a by-stander help to self-reactive $CD8^+$ T cells, whereas Tregs directly suppress priming of $CD8^+$ T cells.

Tregs suppress self-reactive $CD8^+$ T cells via limiting IL-2

Because one of the Treg-mediated effects observed in the previous experiments was the down-regulation of IL-2Rα in OT-I T cells, we hypothesized that Tregs suppress self-reactive $CD8^+$ T cells by limiting IL-2 availability. We observed significantly higher levels of IL-2Rα and pSTAT5, a signaling intermediate of the IL-2 pathway, in OT-I T cells in Treg-deficient mice compared to Treg-replete mice early after priming (Fig. 4A-B, Fig S4A-B). These results were reproduced when congenic Ly5.1 OT-I T cells were used (Fig. S4C-E). These results showed that Tregs limit IL-2 signaling in self-reactive $CD8^+$ T cells in vivo.

Tregs efficiently suppressed proliferation and IL-2Rα expression in $CD8^+$ T cells ex vivo (Fig. 4C). An addition of excessive IL-2 abrogated the suppression of $CD8^+$ T cells by Tregs completely (Fig. 4C). To address whether Tregs can suppress self-reactive $CD8^+$ T cells in the excess of IL-2 in vivo, we performed the diabetic assay with IL-2/anti-IL-2 mAb complexes (IL-2ic) provided during the OT-I priming (Fig. 4D). IL-2ic have markedly increased biological activity in comparison to IL-2 alone [20]. We used IL-2ic with JES6-1A12 antibody clone, promoting IL-2 signaling selectively in T cells expressing high-affinity IL-2Rαβγ trimeric IL-2 receptor, or with S4B6 antibody clone promoting IL-2 signaling irrespective of IL-2Rα expression [20, 21]. Both kinds of IL-2ic broke the peripheral tolerance and induced the onset of autoimmune diabetes similarly to the Treg-depletion (Fig. 4E-F). IL-2ic promoted the formation of OT-I $KLRG1^+$ effector cells (Fig. 4G), although it induced a dramatic expansion of Tregs at the same time (Fig. 4H). Overall, these results showed that Tregs are unable to suppress $CD8^+$ T cells in the excess of IL-2 signal. This strongly supports the hypothesis that the major mechanism of Treg-mediated suppression of self-reactive $CD8^+$ T cells is reducing the IL-2 availability. This mechanism might be specific for suppressing $CD8^+$ T cells, since antigen-activated $CD8^+$ T cells were much more responsive to IL-2 than activated $CD4^+$ T cells (Fig. S4G).

Tregs suppress formation of unique super-effector $CD8^+$ T cells

To study how Treg-mediated suppression changes the gene expression profiles of activated $CD8^+$ T cells, we analyzed the transcriptomes of OT-I T cells primed in the presence or absence of Tregs on a single cell level. Tregs reduced the expression of IL-2 responsive genes, including key cytotoxic molecule granzyme B (GZMB) (Fig. 5A, Fig. S5A-B). Unsupervised clustering high-lighted five different activated OT-I T cell subsets (Fig. 5B). Based on their gene expression profiles (Fig. S5C, Table S1) and comparison with $CD8^+$ T-cell subsets formed during an anti-viral response (Fig. S5D), we identified clusters 0 and 1 as early effector T cells, cluster 2 as memory T cells precursors, and cluster 3 as precursors of exhausted cells.

However, cluster 4 did not match to any established CD8$^+$ T-cell subset. It was characterized by the expression of a natural killer cell activation receptor gene *Klrk1* (alias *Nkg2d*) and *Gzmb* (Fig. 5C, S5C). Interestingly, these cells appeared almost exclusively in the absence of Tregs (Fig. 5D-E). This cluster could be further divided into two subsets, one of them expressing *Ilr7a*, *Cd103*, and natural killer cell markers *Ifitm1-3* and *Cd7*, but not expressing *Cd49d*, encoding a subunit of VLA4 activation marker (Fig. 5F-H, Fig. S5C). Because the unusual co-expression of effector molecules (GZMB, KLRK1) and IL-7Rα might provide superior effector properties to these cells, we called these cells super-effector T cells. In the next step, we validated the results from scRNAseq using flow cytometry and RT-qPCR. This confirmed that KLRK1$^+$ CD49d$^-$ IL-7Rα$^+$ super-effector CD8$^+$ T cells are generated post priming only upon depletion of Tregs (Fig. 5I, S5E). Moreover, the gene expression profile of FACS-sorted super-effector CD8$^+$ T cells matched the original scRNAseq data (Fig. S5F).

Super-effector CD8$^+$ T cells have strong cytotoxic properties

We hypothesized that super-effector CD8$^+$ T cells are induced by excessive IL-2 signals. Indeed, we observed that the depletion of Tregs as well as the administration of IL-2ic induced super-effector T cells in polyclonal mice (Fig. 6A, Fig. S6A-B). Moreover, we observed that the combination of IL-2 administration and antigenic stimulation was most efficient in inducing KLRK1$^+$ CD49d$^-$ super-effector T cells in OT-I mice (Fig. 6B-C, S6C). Surprisingly, only the combination of these two stimuli effectively induced high levels of GZMB and IL-7R (Fig. 6D-F). To address whether super-effector T cells have the hypothesized superior cytotoxic properties, we compared KLRK1$^+$ and conventional KLRK1$^-$ effector T cells from OT-I mice treated with OVA+IL-2ic, and KLRK1$^+$ T cells from mice treated only with OVA in their abilities to kill splenocytes loaded with their cognate antigen *in vivo* (Fig. S6D). KLRK1$^+$ T cells induced by the combination of the antigen and IL-2ic showed the most potent cytotoxic activity on per cell basis (Fig. 6G, Fig. S6E-F).

To identify putative human counterparts of super effector CD8$^+$ T cells, we generated a human blood CD8$^+$ T cells atlas by integrating publicly available single cell transcriptomic data sets. After removing MAIT cells (Fig. S6G, cluster 6), we could identify naïve, memory, and effector T cells, and an unusual population expressing some super-effector signature genes such as *IL7R*, *KLRD1*, *IFITM3,* and *CD7* (Fig. 6H-I, Fig. S6H, Table S2). These human super-effector-like cells constituted for ~1-10% of all CD8$^+$ T cells (Fig. 6J). These cells did not show signs of clonal expansion, but expressed rearranged αβTCR genes excluding that these cells are natural killer cells or another non-T cell subset (Fig. 6K). Because these cells expressed high levels of *IL2RB* (Fig. 6I), a subunit of IL-2 and IL-15 receptors, their gene expression profile was probably modulated by strong IL-2/IL-15 signals, which is in line with the origin of mouse super-effector T cells. Although these cells expressed cytotoxic genes *GNLY* and *GZMK*, the expression of *GZMA* and *GZMB* was

lower in human super-effector-like T cells than in the conventional effector cells (Fig. 6I). This probably reflects the fact that these T cells have not been recently stimulated by their cognate antigen, which is required for the full generation of super-effector cells in mice (Fig. 6B-E). Nevertheless, this previously uncharacterized population of human $CD8^+$ T cells shows striking similarities to mouse super-effector $CD8^+$ T cells induced by supra-physiologic IL-2 levels.

Strong IL-2 signal promotes anti-tumor $CD8^+$ T cells responses

So far, we have documented that Tregs suppress self-reactive $CD8^+$ T cells by limiting IL-2 signal in the context of the autoimmune pathology. We hypothesized that excessive IL-2 signaling may override Treg-mediated suppression of tumor-reactive $CD8^+$ T cells as well. Thus, we investigated the effect of IL-2/JES6 immunocomplexes in a BCL1 leukemia model (Fig. 7A). This IL-2ic slowed down the progression of the disease, when administrated together with a chemotherapeutic drug doxorubicin (Fig. 7B-C, S7A). This effect was dependent on $CD8^+$, but not on $CD4^+$, T cells as revealed by antibody mediated-depletions of these subsets (Fig. 7B). Depletion of $CD4^+$ T cells even improved the anti-tumor effect of doxorubicin plus IL-2ic combinational treatment, presumably due to the depletion of Tregs, which can still limit IL-2 availability in between the IL-2ic injections. The administration of IL-2ic without the chemotherapy did not show any therapeutic effect (Fig. 7B, S7A), suggesting that the combination of the IL-2 signal and antigens released from dead tumor cells was required.

We observed very similar effects of doxorubicin and IL-2/JES6 combinational treatment in a B16F10 melanoma model (Fig. 7D-E, S7B). Since IL-2/JES6 highly selectively stimulates IL-2Rα^+ cells, represented mostly by Tregs in naïve unprimed mice, it was considered as an immunotherapeutic tool for the specific expansion of Tregs in vivo with a potential application in the treatment of autoimmune diseases and pre-transplantation care. On the contrary, our data showed that it promotes anti-tumor responses of $CD8^+$ T cells, particularly in the combination with immunogenic chemotherapy [22], and that this anti-tumor activity was not counteracted by Tregs.

Discussion

In this study, we investigated how Tregs prevent $CD8^+$ T-cell mediated autoimmune pathology. Using a well-controlled system based on the transfer of $CD8^+$ T cells specific for a pancreatic neo-self-antigen, we revealed that regulatory T cells substantially increase the quorum of self-reactive T cells [23] required to induce the autoimmune pathology.

We observed that Tregs do not alter the antigen-affinity discrimination as they suppress both high-affinity and low-affinity $CD8^+$ T cells, which is in an apparent contrast with a previous study [10] concluding that Tregs suppress low-affinity T-cell responses exclusively. The most possible explanation is that the previous study focused on the role of Treg in the $CD8^+$ T-cell response to *Listeria monocytogenes*, where the presence or depletion of Tregs might regulate the kinetics of pathogen clearance and thus the dose of bacterial antigens. Contrary to that, the dose of the priming antigen was constant in our experimental diabetes.

We identified the reduction of available IL-2 as the major mechanism of Treg-mediated tolerance of $CD8^+$ T cells. The evidence is that Treg depletion increases IL-2 signaling in these cells, i.e., pSTAT5 levels and expression of IL-2-responsive genes, and that the administration of IL-2 and IL-2ic mimics the absence of Tregs in vitro and in vivo, respectively. Strong exogenous IL-2 signals stimulate the expansion of Tregs and the expression of their effector molecules [24], which should enhance all their potential suppression mechanisms with the notable exception of sequestering IL-2. However, as these exogenous IL-2 signal mimics the effect of Treg depletion in our model, mechanisms non-targeting IL-2 do not substantially contribute to the suppression of self-reactive $CD8^+$ T cells. This conclusion is in line with some previous studies of Treg-mediated suppression of effector $CD8^+$ T cells [8, 9] and with the importance of IL-2Rα expression in self-reactive $CD8^+$ T cells for the infiltration of pancreatic islets [25]. However, our data show that other proposed mechanisms of Treg-mediated suppression such as inhibiting CD80/CD86 co-stimulation [7, 11], inhibiting the chemokine production by APC [10], or suppressing the production of anti-inflammatory chemokines [12] do not play a major role in the peripheral tolerance of $CD8^+$ T cells. It is still possible that some of these mechanisms indirectly contribute to restricting the IL-2 pool as was proposed for CTLA-4-mediated downregulation of CD80/86 molecules [9]. This might actually explain why we observed a larger effect of Tregs on self-reactive OT-I T cells upon the priming with the (neo)self-antigen than with exogenous mature DCs pre-loaded with the antigenic peptide.

It has been found that the biological activity of IL-2ic is dictated by the clone of the anti-IL-2 mAb [20, 21]. IL-2/JES6 immunocomplexes highly selectively stimulate cells expressing the high-affinity trimeric IL-2 receptor and were considered as an immunosuppressive tool acting via the expansion of Tregs [24]. In

contrast, our conclusion that IL-2 restriction is the major mechanism of Treg-mediated suppression of $CD8^+$ T cells implies that the administration of IL-2/JES6 should release antigen-activated $CD8^+$ T cells from the Treg control. Indeed, IL-2/JES6 in combination with chemotherapy significantly prolonged the survival of tumor-bearing mice in two different tumor models in a $CD8^+$ T-cell-dependent manner. Accordingly, IL-2/JES6 administrated post-priming, but not before the transfer of self-reactive T cells, decreased the T-cell quorum for the induction of experimental diabetes. Collectively, these results reveal that strong sustained IL-2 signal selective for IL-2Rα^+ cells potentiates antigen-induced $CD8^+$ T-cell anti-tumor immunity and autoimmunity despite its concomitant stimulating effects on Tregs.

Our finding that IL-2 restriction is the major mechanism Tregs-mediated regulation of self- and tumor-reactive $CD8^+$ T cells does not exclude the involvement of additional mechanisms for regulating other immune cell types, such as conventional $CD4^+$ T cells. On the contrary, there is substantial evidence that Tregs suppress conventional $CD4^+$ T cells largely via IL-2-independent mechanisms. First, we show that antigen-stimulated $CD4^+$ T cells are less sensitive to IL-2 signals than $CD8^+$ T cells in vivo, which limits the potential impact of the IL-2 restriction on them. Second, it has been shown that Tregs lacking the high-affinity IL-2 receptor, implied in IL-2 sequestration, can still control the homeostasis of $CD4^+$ T cells, but not $CD8^+$ T cells [5]. Third, it has been shown that Treg suppress conventional $CD4^+$ T cells by depleting their cognate peptide-MHCII from APC, which is not applicable for suppressing MHCI-restricted $CD8^+$ T cells [26].

Antigenic stimulation of $CD8^+$ T cells in the presence of excessive IL-2, induced by depletion of Tregs or by the administration of exogenous IL-2R agonists, leads to the formation of a previously uncharacterized subset of T cells, called ‘super-effectors’ here. They express high levels of cytotoxic molecules, such as granzymes, but, unlike conventional effector $CD8^+$ T cells, they also express high levels of IL-7R. Moreover, they express several natural killer receptors including the KLRK1/NKG2D involved in target cell killing [27]. As these cells show superior cytotoxic properties in vivo, blocking their formation is probably the major mechanism of Treg-mediated tolerance of the $CD8^+$ T-cell compartment to healthy and tumor tissues.

Interestingly, antigenic stimulation together with activating antibodies to OX40 and 4-1BB TNF-family receptors induce IL-7Rα^+ effector $CD8^+$ T cells [28]. These cells produce high levels of proinflammatory cytokines in an IL-7-dependent manner [28]. 4-1BB signaling was shown to enhance IL-2 production and IL-2Rα expression in T cells [29, 30], suggesting that the OX40/4-1BB costimulation enhances the IL-2 signaling to alleviate the Treg-mediated suppression. Accordingly, the OX40/4-1BB induced effector $CD8^+$ T cells expressing high levels of IL-2Rα [28]. Interestingly, the authors of this previous study call these

cells 'super-effectors' too. As IL-2-induced and OX40/4-1BB-induced IL-7R$^+$ T cells seam to be very similar, we believe that we can collectively call them 'super-effectors'.

Our reanalysis of publicly available datasets of CD8$^+$ T cells revealed super-effector like CD8$^+$ T cells in the human peripheral blood. These cells show patterns of super-effector T-cell gene expression, but they do not express high levels of cytotoxic molecules, probably because they lack recent antigenic stimulation. Therefore, future studies are needed to resolve the phenotype and function of human super-effector cells. In any case, the potent cytotoxic capacity and their expansion by IL-2 agonists make super-effector cells a promising clinical target in cancer immunotherapy.

Materials and methods

Antibodies, peptides and dyes

Antibodies to the following antigens were purchased from BioLegend and used for flow cytometry: CD4 BV650 (RM4-5, #100545), CD4 Alexa Flour 700 (RM4-5, #100536), CD4 APC-Cy7 (GK15, #100414), CD4 APC (RM4-5, #100516), CD8a BV421 (53-6.7, #100738), CD8a PE (53-6.7, #100708), CD11c Alexa Flour 700 (N418, #117319), CD25 Alexa Fluor 700 (PC61, #102024), CD25 BV605 (PC61, #102036), CD25 BV650 (PC61, #102038), CD25 Pe-Cy7 (PC61, #102016), CD44 BV 650 (IM7, #103049), CD45.1 Alexa Fluor 700 (A20, # 110723), CD45.1 BV650 (A20, #110735), CD45.1 FITC (A20, #110706), CD45.1 PerCP-Cy5.5 (A20, #110728), CD45.2 Alexa Fluor 700 (104, #109822), CD45.2 APC (104, #109814), CD49d APC (R1-2, #103622), CD49d Pe-Cy7 (R1-2, #103618), CD62L FITC (MEL-14, #104406), CD80 PerCP-Cy5.5 (16-10A1, #104722), CD86 Alexa Fluor 700 (GL-1, #105024), CD103 PerCP-Cy5.5 (2 E7, #121416), CD127 PE-Cy7 (A7R34, #135013), TCRβ APC (H57-597, #109212). Antibodies to TCR Vα2 FITC (B20.1, #553288), CD45.1 APC (A20, #558701), CD45.1 PE (A20, #553776), CD49d PE (R1-2, #553157) were purchased from BD Pharmingen. Antibodies to Granzyme B eFluor660 (NGZB, #50-8898-82), FOXP3 PE-Cy7 (FJK-16s, #25-5773-82), FR4 PE/Dazzle594 (12A5, #125016), KLRG1 BV510 (2F1/KLRG1, #138421), KLRK1 PE-eFluor610 (CX5, #61-5882-82), MHC class II (I-A/I-E) FITC (M5/114.15.2, #11-5321-82) were purchased from eBioscience. Anti-TCRβ PE antibody (H57-597, #1146040) was purchased from SONY.

Goat anti-rabbit IgG (H+L) secondary antibody conjugated to Alexa Fluor 647 from Invitrogen (#21245) was used following rabbit anti-mouse phospho-Stat5 (Tyr694) (D47E7) from Cell Signaling (#4322S). Anti-mouse CD3ε antibody (clone 145-2C11, #100302, BioLegend) was used for plate coating.

Anti-CD4 (GK1.5, #BE0003-1) and anti-CD8α (53-6.7, #BE0004-1) depletion antibodies were purchased from Bioxcell (USA).

Anti-mouse IL-2 mAb S4B6 (#BE0043-1) and anti-mouse IL-2 mAb JES6-1A12 (#BE0043) used for preparation of IL-2/S4B6 and IL-2/JES6 complexes, respectively, were purchased from Bioxcell (USA).

OVA (SIINFEKL), Q4R7 (SIIRFERL), and Q4H7 (SIIRFEHL) peptides were purchased from Eurogentec or Peptides&Elephants.

CFSE (#65-0850-84) and Cell Trace Violet (CTV) (#C34557), LIVE/DEAD near-IR (#L10119), and Hoechst 33258 (#H3569) dyes were purchased from Invitrogen.

IL-2/S4B6 and IL-2/JES6 complexes

IL-2/S4B6 and IL-2/JES6 immunocomplexes were described previously [24]. Complexes were prepared by mixing recombinant mouse IL-2 (100 µg/ml; Peprotech) with anti-IL-2 mAb at a molar ratio of 2:1 in PBS. After 15 min incubation at room temperature, the complexes were diluted in PBS into the desired concentration, frozen at -20 °C, and thawed shortly before application.

Mice

All the mice had C57Bl/6J or BALB/C background. DEREG [15], *FOXP3*^{DTR} [16], RIP.OVA [14], OT-I *Rag2*$^{-/-}$ [31], OT-II *Rag2*$^{-/-}$ [32], Ly5.1 [33] strains were described previously. Mice were bred in specific-pathogen-free facilities (Institute of Molecular Genetics of the Czech Academy of Sciences, Prague; Department of Biomedicine, University Hospital, Basel) or in a conventional facility (Institute of Microbiology of the Czech Academy of Sciences, Prague). Animal protocols were performed in accordance with the laws of the Czech Republic and Cantonal and Federal laws of Switzerland, and approved by the Czech Academy of Sciences or the Cantonal Veterinary Office of Baselstadt, Switzerland, respectively.

Males and females were used for the experiments. At the start of the experiment, all mice were 6-11 weeks old. If possible, age- and sex-matched pairs of animals were used in the experimental groups. If possible, littermates were equally divided into the experimental groups. No randomization was performed when the experimental groups were based on the genotype of the mice; otherwise mice were assigned to experimental groups randomly (defined by their ID numbers) prior to the contact between the experimenter and the mice. The experiments were not blinded since no subjective scoring method was used.

RT-qPCR

2-10 × 10^4 OT-I T lymphocytes were FACS sorted as CD8$^+$ CD45.1$^+$ CD49d$^-$ KLRK1$^-$ cells (naïve), CD8$^+$ CD45.1$^+$ CD49d$^+$ KLRK1$^-$ cells (antigen experienced), CD8$^+$ CD45.1$^+$ CD49d$^+$ KLRK1$^+$ cells (double positive), or CD8$^+$ CD45.1$^+$ CD49d$^-$ KLRK1$^+$ cells (SE). Total RNA was isolated by TRIzol LS (Invitrogen, #10296010) and in-column DNase digestion using RNA Clean & Concentrator Kit (Zymo Research), according to manufacturers' instructions. RNA was stored at -80 ºC or transcribed immediately using RevertAid reverse transcriptase (Thermo Fisher Scientific, #EP0442) with oligo(dT)18 primers according to the manufacturer's instructions. RT-qPCR was carried out using LightCycler 480 SYBR green I master chemistry and a LightCycler 480 machine (Roche). All samples were measured in triplicates. Median CT values were normalized to a reference gene, Glyceraldehyde-3-Phosphate Dehydrogenase (*Gapdh*). The sequences of used primers are:

Gapdh: F TGCACCACCAACTGCTTAGC, R GGCATGGACTGTGGTCATGAG

mCd7: F TGGATGCCCAAGACGTACA, R TAAGATCCCTTCCAGGTGCC

mIfitm1: F ATGCCTACTCCGTGAAGTCTAGG, R GACAACGATGACGACGATGGC

mGzma: F AAAGGACTCCTGCAATGGGG, R ATCGGCGATCTCCACACTTC

mGzmb: F GGGGCCCACAACATCAAAGA, R GGCCTTACTCTTCAGCTTTAGCA

mGzmk: F AAGGATTCCTGCAAGGGTGA, R ATTCCAGGCTTTTTGGCGATG

mKlrd1: F TCGGTGGAGACTGATGTCTG, R AACACAGCATTCAGAAACTTCC

mIl7r: F AAAGCCAGAGCGCCTGGGTG, R CTGGGCAGGGCAGTTCAGGC

mIl2ra: F AGAACACCACCGATTTCTGG, R GGCAGGAAGTCTCACTCTCG

mCxcr6: F ACTGGGCTTCTCTTCTGATGC, R AAGCGTTTGTTCTCCTGGCT

Enrichment of T lymphocytes

T lymphocytes were enriched by negative selection using the Dynabeads Biotin Binder kit (Invitrogen, #11047), and biotinylated anti-CD19 (clone 1D3, ATCC# HB305), anti-CD4 (clone YTS177), or anti-CD8 antibodies (clone 2.43, ATCC# TIB-210), depending on the experimental setup. Antibodies were produced and biotinylated in house using (+)-Biotin N-hydroxysuccinimide ester (Sigma Aldrich) in bicarbonate buffer. The excessive biotin was separated from the antibody using Sephadex G-25 (Sigma Aldrich). For RT-qPCR experiments, $CD8^+$ T cells were enriched using Dynabeads Untouched Mouse CD8 Cells Kit (Invitrogen, #11417D) according to manufacturer's instructions.

Flow cytometry and cell sorting

Live cells were stained with relevant antibodies on ice. LIVE/DEAD near-IR dye or Hoechst 33258 were used for discrimination of viable and dead cells.

For intracellular staining of FOXP3 and Granzyme B, cells were fixed and permeabilized using Foxp3 / Transcription Factor Staining Buffer Set (#00-5523-00, Invitrogen) according to the manufacturer's instructions. Fixed cells were stained at room temperature for 1 h.

For intracellular staining of pSTAT5, splenic cells were fixed using Fixation/ Permeabilization buffer (Foxp3 / Transcription Factor Staining Buffer Set, #00-5523-00, Invitrogen) at room temperature for 15 min, washed twice with Permeabilization buffer (Foxp3 / Transcription Factor Staining Buffer Set, #00-5523-00, Invitrogen), washed with PBS and stained with anti-pSTAT5 antibody at room temperature overnight. The next day, cells were stained with secondary antibody at room temperature for 1 h.

Flow cytometry was carried out using an LSRII (BD Bioscience) or an Aurora (Cytek). Data were analyzed using FlowJo software (BD Bioscience).

Cell sorting was performed on an Influx or an Aria machines (both BD Bioscience).

ELISA

The anti-idiotypic B1 mAb was produced by the use of B1 hybridoma via the conventional ascites producing approach in parafine oil pre-treated BALB/C mice. It was purified by 45% supercritical antisolvent precipitation (ammonium sulphate) followed by extensive dialysis against distilled water, centrifuged at 12000 g for removal of IgM, and purified by a protein A affinity chromatography. Next, it was biotinylated with Sulpho NHS-biotin reagent (Pierce) according to the manufacturer´s protocol. Blood of mice was taken on day 54 of B-cell leukemia/lymphoma experiment. Blood serum was separated and serially diluted (1:40 – 1:640) in PBS. Plate wells (Costar) were coated with 50 µl of diluted samples and incubated overnight at 4 °C, followed by blocking with 1% gelatin (200 µl per well, 2 h at room temperature). Biotinylated anti-idiotypic B1 mAb was added (20 ng/ml) in a buffer containing 0.5% gelatin, 3% PEG, and 0.1% tween, and plate was incubated for 2 h at room temperature. Next, samples were conjugated with ExtrAvidin−Peroxidase (Sigma-Aldrich) for 1 h at room temperature, and 3,3′,5,5′-tetramethylbenzidine substrate (Sigma-Aldrich) was added for 10 min in dark. Reaction was stopped with 50 µl of 2M H_2SO_4, and absorbance at 450 nm was measured by a Biolisa spectrometer (Bioclin).

Bone marrow-derived dendritic cells

Bone marrow cells were seeded on 100 mm plates (tissue culture untreated) and maintained in DMEM (Sigma Aldrich) containing 10% FBS (GIBCO), 100 U/ml penicillin (BB Pharma), 100 mg/ml streptomycin (Sigma Aldrich), 40 mg/ml gentamicin (Sandoz), and 2% of supernatant from J558 cells producing GM-CSF for 10 days at 5% CO_2 at 37 °C [34]. The cells were split every 2-3 days. On day 10, cells were incubated in the presence of 100 ng/ml LPS (Sigma Aldrich) and 200 nM of indicated peptide for 3 h at 5% CO_2 at 37 °C. Next, plates were incubated with 0.02% EDTA in PBS for 5 min at 5% CO_2 at 37 °C, and harvested. Washed and filtered cells were used for adoptive transfers.

In vitro proliferation assay

$CD8^+$ T lymphocytes from WT mice were FACS sorted, labeled with CTV, and plated into an anti-CD3ε-antibody-coated 48-well plate in IMDM (10% FBS (GIBCO), 100 U/ml penicillin (BB Pharma), 100 mg/ml streptomycin (Sigma Aldrich), 40 mg/ml gentamicin (Sandoz)). Tregs, sorted as $CD4^+$ GFP^+ T lymphocytes from $DEREG^+$ mice were added to corresponding wells of the plate in 1:1 ratio with conventional $CD8^+$ T

lymphocytes. Recombinant IL-2 (2 ng/ml) was added or not. Cells were incubated at 37°C, 5% CO2 for 72 h and analyzed by flow cytometry.

In vivo proliferation assay

OT-I CD8$^+$ and OT-II CD4$^+$ T cells were isolated from OT-I *Rag2*$^{-/-}$ and OT-II *Rag2*$^{-/-}$ mice, respectively, using MACS negative selection kits. On day 0, mixture of OT-I CD8$^+$ (0.75×10^6 cells) and OT-II CD4$^+$ (1.5×10^6 cells) CFSE labeled cells was adoptively transferred into recipient Ly5.1 mice. The next day, recipient mice were immunized with ovalbumin protein i.p. (75 µg/mouse), and after 6 h, they received the first dose of IL-2ic (1.5 µg IL-2 equivalent/dose, i.p). On days 2, 3, and 4 mice received additional IL-2ic doses. On day 5 post-immunization, spleens of Ly5.1 mice were collected and used for flow cytometry analysis.

Treg depletion

In order to deplete Tregs, 0.25 µg of DT (#D0564, Sigma-Aldric) was administered i.p. to DEREG$^+$ RIP.OVA mice and control DEREG$^-$ RIP.OVA mice for two consecutive days.

Model of autoimmune diabetes

The model of autoimmune diabetes has been described previously [13]. Briefly, an indicated number of OT-I T cells isolated from OT-I *Rag2*$^{-/-}$ mice were adoptively transferred into a recipient RIP.OVA mouse i.v. On the following day, the recipient mice were immunized with 10^6 of bone marrow-derived dendritic cells loaded with indicated peptide (i.v.) or with 25 µg LPS + 50 µg OVA peptide in 200 µl PBS (i.p.).

Alternatively, *Cd3ε*$^{-/-}$ RIP.OVA recipient mice received 10^6 of polyclonal CD8$^+$ T lymphocytes derived from RIP.OVA Ly5.1 donors 8 days prior to immunization. One day prior to immunization, *Cd3ε*$^{-/-}$ RIP.OVA mice received 4-8 × 10^5 Tregs (sorted as CD4$^+$ GFP$^+$ TCRβ$^+$) or 10^6 conventional CD4$^+$ T lymphocytes (sorted as CD4$^+$ GFP$^-$ TCRβ$^+$) derived from DEREG RIP.OVA donors.

If IL-2ic were used, 1.5 µg IL-2 equivalent/dose of IL-2/S4B6 or IL-2/JES6 were injected i.p. on day 0, 1, and 2 post-immunization. Alternatively, mice received 5 doses of IL-2/JES6 (2.5 µg IL-2 equivalent) on days -7, -6, -5, -4, -3 prior to the immunization.

Urine glucose was monitored on a daily basis using test strips (GLUKOPHAN, Erba Lachema). Blood glucose was measured using Contour blood glucose meter (Bayer) on a day 7, 8, or 14 post-immunization, depending on the experimental design. The animal was considered diabetic when the concentration of glucose in the urine reached ≥ 1000 mg/dl for two consecutive days.

Induction of SE cells using IL-2ic

On day 0, recipient mice (OT-I Rag2$^{-/-}$ or RIP.OVA) received 25 µg OVA peptide in 200 µl of PBS and/or 0.75 µg IL-2 equivalent/dose of IL-2/S4B6 in 250 µl PBS i.p. On days 1 and 2, mice received 2 more doses of IL-2/S4B6. On day 3, spleens were collected, and used for flow cytometry analysis or FACS sort.

In vivo killing assay

In vivo CD8$^+$ T cell killing assay was performed as described previously [35] with minor modifications. In short, OT-I *Rag2*$^{-/-}$ mice were immunized or not with OVA peptide (25 µg, single dose on day 0, i.p.) and/or IL-2/S4B6 (0.75 µg IL-2 equivalent/dose of IL-2/S4B6, 3 doses, days 0-2, i.p.). On day 3, FACS sorted KLRK1$^+$ CD8$^+$ or KLRK1$^-$ CD8$^+$ cells were injected i.v. to recipient RIP.OVA mice, which had received a mixture of target cells (10^7 OVA-pulsed cells and 10^7 unpulsed target cells) earlier the same day. Target cells were prepared from spleens of Ly5.1 mice. OVA-pulsed cells were prepared via 1 h incubation in RPMI-1640 containing 10% FBS (GIBCO), 100 U/ml penicillin (BB Pharma), 100 mg/ml streptomycin (Sigma Aldrich), 40 mg/ml gentamicin (Sandoz), and 2 µM OVA peptide at 37°C, 5% CO_2, followed by loading with CTV. Unpulsed target cells were incubated in parallel in the medium without OVA peptide, and subsequently loaded with CFSE. On day 4, splenocytes of the recipient mice were analyzed by flow cytometry. Target cells were identified as CD45.1$^+$ cells. Ratio of unpulsed (CFSE$^+$) to OVA pulsed target cells (CTV$^+$) was determined and normalized to those of recipients which did not receive OT-I T cells.

Murine B-cell leukemia

On day 0, BALB/C female mice were injected i.p. with 5×10^5 BCL1 cells (a BALB/c-derived leukemia cell line) [36] in PBS. On days 11 and 24 post-inoculation, mice received doxorubicin (Adriblastina) (5 mg/kg in 250 µl PBS, i.v.), followed or not by anti-CD4 or anti-CD8α depletion mAbs (200 µg in 250 µl of PBS for both, i.p.). On days 12, 13, 14, 25, 26, and 27 IL-2/JES6 was administrated to mice (5 µg IL-2 equivalent/dose in 250 µl PBS, i.p.). Survival of mice was monitored from day 30 to day 100. On days 28, 54, and 64-96 blood serum of mice was used for ELISA for antibody against the idiotype of IgM expressed on the BCL1 cells.

B16F10 melanoma

Female C57Bl/6J mice were inoculated s.c. with 5×10^5 B16F10 melanoma cells (day 0). On day 6, mice received doxorubicin (Adriblastina) (8 mg/kg in 250 µl PBS, i.v.) followed or not by anti-CD8α or anti-CD4 depletion mAbs (200 ug in 250 µl of PBS, i.p.). On days 7, 8, and 9 IL-2/JES6 was injected to mice (5 µg IL-2 equivalent/dose in 250 µl PBS, i.p.). Survival of mice was monitored on a daily basis.

ScRNA sequencing

Six weeks old female DEREG^{-} RIP.OVA (n=3) and DEREG^{+} RIP.OVA (n=3) littermate mice were treated with DT (0.250 µg per mouse in 0.5 ml of PBS, i.p.) on days -2 and -1 prior to the immunization, followed by i.v. injection of 5×10^4 OT-I T cells in 200 µl of PBS on day -1. OT-I T cells were obtained from spleens and lymph nodes of Ly5.1 OT-I *Rag2*$^{-/-}$ mouse. On day 0, mice received Ly5.1 dendritic cells loaded with OVA (10^6 cells per mouse in 200 µl of PBS). On day 3 post-immunization, mice were sacrificed and spleens were collected. Erythrocytes were lysed with ACK buffer (2 min, on ice), cells were washed and resuspended in PBS/ 2% FBS. Next, cells were stained with LIVE/DEAD near-IR dye, anti-CD8a BV421, anti-CD45.1 PE, and anti-CD45.2 APC antibodies together with TotalSeq-C anti-mouse hashtag antibodies (anti-CD45 clone 30-F11, anti-H-2 clone M1/42, Biolegend, #155869 (MH5), #155871 (MH6), #155873 (MH7), #155875 (MH8), #155877 (MH9) and #155879 (MH10)). Viable CD8a^{+}, CD45.1^{+}, CD45.2^{-} OT-I cells were FACS sorted. The individual samples were pooled together and with cells coming from an unrelated experiment. These unrelated cells were labeled with unique hashtag antibodies and removed during the analysis. The viability and concentration of cells after sort were measured using the TC20 Automated Cell Counter (#1450102, Bio-Rad). The viability of the cells pre-loading was > 90%. Cells were loaded onto a 10x Chromium machine (10x Genomics) aiming at the yield of 1000 cells per sample and processed with Feature Barcode technology for Cell Surface Protein protocol (#CG000186 Rev D) with the Chromium Single Cell 5' Library & Gel Bead and Chromium Single Cell 5' Feature Barcode Library kits (10x Genomics, #PN-1000014, #PN-1000020, #PN-1000080, #PN-1000009, #PN-1000084). Resulting cDNA libraries were sequenced on a NovaSeq 6000 (Illumina) with the S1 Reagent Kit (100 or 300 cycles, Illumina, #20012865, #20012863).

Analysis of scRNAseq data

The raw scRNA data were mapped to Mouse Reference GRCm38 obtained from Ensembl database v102 [37] by 10x Genomics Cell Ranger 5.0.0 [38]. The same software was also used to create the employed mouse transcriptome reference. Default parameters were kept.

The hashtag sequences were mapped using the hashtag sequence references by 10x Genomics Cell Ranger 5.0.0. The data were pre-processed using Seurat R package v4.0.3 [39] on R v4.0.4 (https://www.r-project.org/). The cells with less than 200 transcripts were removed. A histogram of cell counts having a specified number of hashtag reads was computed for each hashtag. To detect the end of an initial slope of a histogram, a function based on descent along the gradient – moving to the neighboring point in the histogram as long as its associated value is lower - was used. Before its application, each histogram was averaged using the sliding window of size n = 5 points. The resulting limit was used to associate or not each

cell with the respective sample. Cells marked by multiple hashtags were considered as doublets and excluded from further analysis. Read limits (lim) and the number of recovered cells (#) for individual hashtags were: MH6 (lim 19, #778), MH7 (lim 24, #789), MH8 (lim 21, #849), MH9 (lim 35, #836), MH10 (lim 25, #878).

The lists of barcodes of each uniquely marked cell were created and used to separate read pairs where the start of first read R1 matches one of barcodes exactly from those with different barcodes and consequently either originating from the cells from unrelated experiment, from cell doublets or insufficiently marked cells. These reads were mapped again using 10x Genomics Cell Ranger 5.0.0 to generate data used further for downstream analysis. Cells with less than 200 transcripts and/or more than 15 % of transcripts mapping to mitochondrial genes were removed. Mitochondrial genes, TCRα and TCRβ V(D)J-genes, ribosomal genes and genes whose transcripts were detected in less than three cells were excluded. Log normalization (scale factor = 1×10^4), scaling, identification of variable features (2000 variable features), dimensional reduction (PCA and UMAP with top 50 and 15 principal components respectively, 40 nearest neighbors for UMAP), identification of nearest neighbors in the reduced space ('rann' algorithm) and Louvain clustering (resolution = 0.8) were performed using the Seurat R package v4.0.3 [39] on R v4.0.4 (https://www.r-project.org/). These steps allowed to identify the low-quality cells and contaminating cell types that were removed along with cells with more than 7.5% of transcripts mapping to mitochondrial genes. In total, 4043 cells passed the QC steps. Afterwards, all steps starting from and including log-normalization were repeated using slightly different parameters (800 variable features, 12 top principal components for both UMAP and PCA dimensional reductions and 30 nearest neighbors for UMAP, resolution = 0.3 for Louvain clustering; other parameters stayed the same). Cell cycle scores for S phase and G2/M phases were regressed out in the scaling step. Projection of clusters on a reference dataset of acute and chronic viral infection $CD8^+$ T cells was done using the ProjecTILs R package v0.6.0 [40]. For the separate analysis of super effector cells, cluster 4 was extracted from the original data and re-clustered again with adjusted parameters.

The code for the cell filtration to hashtags, barcode extraction and whole downstream analysis is accessible on GitHub (https://github.com/Lab-of-Adaptive-Immunity/Supereffectors_scRNAseq).

Gene set enrichment analysis

Lists of IL-2 responsive genes were obtained from literature [41, 42]. Fold changes between $DEREG^+$ and $DEREG^-$ samples were calculated with the Seurat R package v4.0.3 [39]. Gene set enrichment analysis (GSEA) analysis was performed using the fgsea R package v1.16.0 [43]. Genes with similar fold changes were ranked in a random order.

Building and analysis of Human CD8$^+$ T-cell atlas

The Human CD8$^+$ Atlas was built from 14 different data sets previously mapped to human genome reference GRCh38 by 10x Genomics and downloaded from their support site (https://support.10xgenomics.com/) either as raw feature matrices or, if not available for given data set, as filtered feature matrices. For data sets with available V(D)J information their list was downloaded either as list of filtered annotated contigs or, if not available for given data set or it was originally procesed by Cell Ranger 5.0.0 or higher, as list of all annotated contigs. The following data sets were used: *CD8$^+$ T cells of Healthy Donor 1*, Single Cell Immune Profiling Dataset by Cell Ranger 3.0.2, 10x Genomics, (2019, May 9); *CD8$^+$ T cells of Healthy Donor 2*, Single Cell Immune Profiling Dataset by Cell Ranger 3.0.2, 10x Genomics, (2019, May 9); *CD8$^+$ T cells of Healthy Donor 3*, Single Cell Immune Profiling Dataset by Cell Ranger 3.0.2, 10x Genomics, (2019, May 9); *CD8$^+$ T cells of Healthy Donor 4*, Single Cell Immune Profiling Dataset by Cell Ranger 3.0.2, 10x Genomics, (2019, May 9); *10k Human PBMCs with TotalSeq-B Human TBNK Antibody Cocktail, 3' v3.1*, Single Cell Gene Expression Dataset by Cell Ranger 6.0.0, 10x Genomics, (2021, March 31); *10k Human PBMCs Multiplexed, 2 CMOs - Inputs/Library*, Single Cell Gene Expression Dataset by Cell Ranger 6.0.0, 10x Genomics, (2021,March 2); *5k Peripheral blood mononuclear cells (PBMCs) from a healthy donor (v3 chemistry)*, Single Cell Gene Expression Dataset by Cell Ranger 3.0.2, 10x Genomics, (2019, May 29); *10k PBMCs from a Healthy Donor - Gene Expression and Cell Surface Protein*, Single Cell Gene Expression Dataset by Cell Ranger 3.0.0, 10x Genomics, (2018, November 19); *8k PBMCs from a Healthy Donor*, Single Cell Gene Expression Dataset by Cell Ranger 2.1.0, 10x Genomics, (2017, November 8); *PBMCs of a Healthy Donor (v1)*, Single Cell Immune Profiling Dataset by Cell Ranger 3.1.0, 10x Genomics, (2019, July 24); *Human T cells from a Healthy Donor, 1k cells - multi (v2)*, Single Cell Immune Profiling Dataset by Cell Ranger 5.0.0, 10x Genomics, (2020, November 19); *Human PBMC from a Healthy Donor, 10k cells - multi (v2)*, Single Cell Immune Profiling Dataset by Cell Ranger 5.0.0, 10x Genomics, (2020, November 19); *Human PBMC from a Healthy Donor, 1k cells (v2)*, Single Cell Immune Profiling Dataset by Cell Ranger 4.0.0, 10x Genomics, (2020, August 25); and *PBMCs of a healthy donor - 5' gene expression and cell surface protein*, Single Cell Immune Profiling Dataset by Cell Ranger 3.0.0, 10x Genomics, (2018, November 19).

Cells with less than 200 transcripts, above-average transcript count plus identified as doublets by scds R package v1.4.0 [44] on R v4.0.4 (https://www.r-project.org/), and/or cells with more than 10% transcripts mapping to mitochondrial genes were removed. The genes equivalent to those removed in our mouse data set plus V(D)J genes of TCRγ and TCRδ genes were excluded. Centered log-ratio normalization of cell surface protein counts for data sets that have them, log-normalization (scale factor = 1×10^4) and identification of variable features for each data set (2500 variable features) were performed using Seurat R

package v4.0.0 [39]. The same package was used for the integration of all data sets and subsequent scaling, dimensional reduction (PCA and UMAP with top 20 principal components), nearest neighbors identification and Louvain clustering (resolution = 0.4) of the resulting data set. The newly emerging cluster of cells with below-average gene count and above-average proportion of transcripts mapping to mitochondrial genes was removed. In total, 140,564 cells passed the QC steps. Afterwards, the previous steps starting from and including both normalizations were repeated using the same parameters. A cluster containing 5,160 MAIT cells was identified using differential expression analysis and V(D)J information, which was kept for some analyses, but removed for others. OPTICs method from dbscan R package v1.1-6 [45] was applied (parameters minPts = 500 and eps_cl = .55 for data both with and without MAIT cells) to generate the final clustering.

The code for building the atlas and its whole analysis is available on GitHub (https://github.com/Lab-of-Adaptive-Immunity/HS-CD8-Atlas).

Author Contribution

OS conceived the study. OT, TC, JK, IM, SJ, HR, AD, HV, VG, MK, and OS performed experiments. OT, TC, JK, IM, SJ, MK, and OS analyzed experiments. VN and JM analyzed scRNAseq data. OT, VN, JM, and OS wrote the first draft. All authors reviewed and commented on the manuscript.

Conflict of Interest

All authors declare that they have no conflict of interest.

Acknowledgement

This study was supported by ERC Starting Grant (FunDiT to OS), Czech Science Foundation (19-03435Y to OS and 18-12973S to MK), Purkyne Fellowship of the Czech Academy of Sciences (to OS), Research Fund for Young Scientists at the University of Basel (DMS2336 to OS), the Institute of Molecular Genetics of the Czech Academy of Sciences (RVO 68378050 to OS), the Institute of Microbiology of the Czech Academy of Sciences (RVO 61388971 to MK), and Charles University Grant Agency (1706119 to OT and TC). The animal facility of the Institute of Molecular Genetics is a part of the Czech Center for Phenogenomics supported by the Czech Ministry of Education, Youth and Sports and the European Regional Development Fund (LM2015040, LM2018126, OP RDI CZ.1.05/2.1.00/19.0395, OP RDI BIOCEV CZ.1.05/1.1.00/02.0109).

VN and SJ are students of the Faculty of Science, Charles University in Prague.

Figure legends

Figure 1

A. Scheme of RIP.OVA diabetes model. OT-I T cells were transferred into *Foxp3*^{DTR} RIP.OVA or DEREG RIP.OVA mice (Treg-depleted with DT) and RIP.OVA controls (Treg-replete). The next day, mice were immunized with OVA peptide and LPS. Urine glucose levels were monitored on a daily basis for 14 days.

B-D. Diabetes was induced in RIP.OVA mice as described in A. **B.** Percentage of diabetic mice is shown. Number of diabetic mice and total number of mice per group is indicated on top of each column. Number of transferred OT-I T cells is indicated for each group. **C.** Glucose concentration in blood on day 7 post-immunization is shown. RIP.OVA n=19, DEREG RIP.OVA n=9, *Foxp3*^{DTR} RIP.OVA n=9. One mouse from *FOXP3*^{DTR} RIP.OVA group died before the measurement (shown as "x"). **D.** Diabetes was induced in RIP.OVA (Ly5.1/Ly5.2, n=4) and *Foxp3*^{DTR} RIP.OVA (Ly5.1, n=7) mice using 0.5×10^6 OT-I T cells. Spleens were collected on day 5 and analyzed by flow cytometry. Percentage of OT-I T cells in CD8$^+$ T-cell population is shown.

E-F. RIP.OVA (Ly5.1/Ly5.2), *Foxp3*^{DTR} RIP.OVA (Ly5.1), DEREG RIP.OVA (Ly5.1/Ly5.2), and *Foxp3*^{DTR} (Ly5.1) mice were treated as shown in A, with the exception that on day 0, mice were stimulated with LPS only (without OVA peptide). **E.** Percentage of diabetic mice is shown. Number of diabetic mice and total number of mice per group is indicated on top of each column. Number of transferred OT-I T cells is indicated for each group. **F.** Diabetes was induced using 0.5×10^6 OT-I T cells. Spleens were collected on day 5 and analyzed by flow cytometry. Left: percentage of OT-I T cells in CD8$^+$ T-cell population is shown. RIP.OVA n=5, *Foxp3*^{DTR} RIP.OVA n=9, *Foxp3*^{DTR} n=8. Right: percentage of effector cells defined as CD44$^+$ CD62L$^-$ in OT-I T-cell population is shown. RIP.OVA n=4, *Foxp3*^{DTR} RIP.OVA n=9, *Foxp3*^{DTR} n=8.

Statistical significance was calculated by Kruskal-Wallis test (p-value is shown in italics) with Dunn's post-test (* <0.05, **<0.01) for comparison of three groups (C, F), or two-tailed Mann-Whitney test for comparison of two groups (D, p-value shown in italics). Median is shown.

Figure 2

A-C. Treg-depleted DEREG$^+$ RIP.OVA mice and control DEREG$^-$ RIP.OVA mice received indicated numbers of OT-I T cells (10^3 or 3×10^2 OT-I T cells in **A**, 3×10^4 OT-I T cells in **B**, 10^6 OT-I T cells in **C**). The next day, mice were immunized with DC loaded with an indicated peptide (OVA in **A**, Q4R7 in **B**, Q4H7 in **C**). Urine glucose level was monitored on a daily basis for 14 days. **A.** Left: Percentage of diabetic mice is shown. Number of diabetic mice and total number of mice per group is indicated on top of each

column. Middle: Survival curve. Number of mice per group is indicated. Right: Blood glucose concentration on day 7 post-immunization. **B-C.** Left: Survival curve. Number of mice per group is indicated. Right: Blood glucose concentration on day 7 post-immunization.

D-F. Diabetes was induced in DEREG$^-$ RIP.OVA and DEREG$^+$ RIP.OVA mice similarly to A-C. On day 6, spleens were collected and analyzed by flow cytometry. Percentage of OT-I T cells among CD8$^+$ T cells, count of KLRG1$^+$ OT-I T cells, and count of IL-2Rα$^+$ OT-I T cells are shown. **D.** Diabetes was induced using DC-OVA and 10^3 OT-I T cells. Left: DEREG$^-$ n=9, DEREG$^+$ n=10. Middle: DEREG$^-$ n=7, DEREG$^+$ n=9. Right: n=5 mice per group. **E.** Diabetes was induced using DC-Q4R7 and 3×10^4 OT-I T cells. Left: DEREG$^-$ n=13, DEREG$^+$ n=10. Middle: DEREG$^-$ n=10, DEREG$^+$ n=9. Right: DEREG$^-$ n=6, DEREG$^+$ n=7. **F.** Diabetes was induced using DC-Q4H7 and 10^6 OT-I T cells, n=8 mice per group.

G-H. RIP.OVA mice were treated or not with IL-2/JES6 for five consecutive days. Two days after the last dose, the mice received 10^3 OT-I T cells, and the next day they were immunized with DC-OVA. Urine glucose level was monitored on a daily basis for 14 days. **G.** Experimental scheme. **H.** Left: Survival curve. Right: Blood glucose concentration on day 7 post-immunization. n=12 mice per group.

Statistical significance was calculated by Log-rank (Mantel-Cox) test (survival) or two-tailed Mann-Whitney test (glucose concentration and flow cytometry analysis). P-value is shown in italics. Median is shown.

Figure 3

Cd3ε$^{-/-}$ RIP.OVA mice received 10^6 polyclonal CD8$^+$ T cells from Ly5.1 RIP.OVA mice. After seven days, they received either 10^6 conventional CD4$^+$ T cells (GFP$^-$), or 0.4-1 $\times$ 10^6 Tregs (GFP$^+$) from DEREG$^+$ RIP.OVA mice, or no CD4$^+$ T cell transfer (NT). Next, 250 OT-I T cells were adoptively transferred to all the recipients. Next day, mice were immunized with DC-OVA.

A. Experimental scheme.

B-C. Urine glucose level was monitored on a daily basis until day 21 post-immunization. **B.** Survival curve. Number of mice is indicated. **C.** Blood glucose concentration on day 8 and day 14 post-immunization is shown. Day 8: NT n=28, Conv. CD4$^+$ n=25, Tregs n=15. Day 14: NT n=15, Tregs n=8.

D-G. On day 8 or day 14, spleens were collected and analyzed by flow cytometry. Percentage of OT-I T cells among CD8$^+$ T cells (**D, F**), and count of KLRG1$^+$ OT-I T cells (**E, G**) are shown. Day 8: NT n=25, Conv. CD4$^+$ n=15, Tregs n=12. Day 14: NT n=15, Tregs n=7.

Statistical significance was calculated by Kruskal-Wallis test (p-value is shown in italics) with Dunn's post-test (* <0.05, **<0.01, ***<0.001) for comparison of three groups, or two-tailed Mann-Whitney test for comparison of two groups (p-value is shown in italics). Median is shown.

Figure 4

A-B. OT-I T cells (5×10^4) were transferred into Treg-depleted DEREG$^+$ RIP.OVA mice and control DEREG$^-$ RIP.OVA mice. The next day, mice were immunized with DC-OVA. On day 3 post-immunization, spleens were collected and analyzed by flow cytometry. OT-I T cells were identified as OVA-tetramer and TCRVα2 double positive. **A.** IL-2Rα expression on OT-I T cells. Left: a representative experiment out of 3 in total. Right: n=5 mice per group. **B.** pSTAT5 expression in OT-I T cells. Left: a representative experiment out of 3 in total. Right: Geometric mean fluorescence intensity (MFI) of anti-pSTAT5-Alexa Fluor 647 in OT-I T cells. Mean of MFI values for each group per experiment are shown as a grey dots. Lines connect data from corresponding experiments. DEREG$^-$ n=7, DEREG$^+$ n=6.

C. In vitro proliferation assay. CTV-labelled CD8$^+$ T lymphocytes were stimulated with plate-bounded anti-CD3ε-antibody in the presence or absence of Tregs and/or recombinant IL-2. After 72 h, cells were analyzed by flow cytometry. Left: Proliferation is indicated by the CTV dilution. Right: IL-2Rα expression on CD8$^+$ T cells. A representative experiment out of 4 in total.

D-F. Treg-depleted DEREG$^+$ RIP.OVA mice and control DEREG$^-$ RIP.OVA mice received OT-I T cells, followed by the immunization with OVA peptide and LPS. On days 0, 1, and 2 post-immunization, RIP.OVA mice received IL-2ic (IL-2/S4B6 or IL-2/JES6). **D.** Experimental scheme. **E-F.** Urine glucose level was monitored on a daily basis for 14 days. Number of mice is indicated. Four mice from IL-2/JES6 group died before day 5 and were excluded from the analysis **E.** Survival curve is shown. **F.** Blood glucose concentration on day 7 post-immunization.

G-H. Diabetes was induced in Treg-depleted DEREG$^+$ RIP.OVA mice (with DT) or Treg-replete DEREG$^+$ RIP.OVA mice (without DT), which later received IL-2ic (IL-2/S4B6 or IL-2/JES6), or were left untreated (control) (scheme D). On day 5 post-immunization, spleens were collected and analyzed by flow cytometry. Four mice from IL-2/JES6 group died before the analysis (shown as "x"). Control n=6, IL-2/S4B6 n=6, IL-2/JES6 n=2, DEREG$^+$ DT n=4. **G.** Number of KLRG1$^+$ OT-I T cells. **H.** Number of Tregs (defined as GFP$^+$ CD4$^+$ T cells).

Statistical significance was calculated by two-tailed Mann-Whitney test (comparison of two groups), Kruskal-Wallis test (comparison of four groups), or Log-rank (Mantel-Cox) test (survival), p-value is shown in italics. Median is shown.

Figure 5

A-E. Ly5.1 OT-I T cells were adoptively transferred into Treg-depleted DEREG$^+$ RIP.OVA and control DEREG$^-$ RIP.OVA mice (n=3 mice per group). The next day, mice were immunized with DC-OVA. On day 3 post-immunization, spleens were isolated and OT-I T cells were FACS sorted as Ly5.1$^+$ CD8$^+$ cells, and analyzed via scRNAseq.

A. Heat map showing the relative expression of canonical IL-2 responsive genes**.** Each column represents one mouse.

B-D. UMAP projection of the individual OT-I T cell based on their gene expression profile. **B.** The colors indicate individual clusters revealed by unsupervised clustering. **C.** The intensity of the blue color indicates the level of *Klrk1* expression in individual cells. **D.** The origin of the cells (DEREG$^+$ or DEREG$^-$ mice) is indicated.

E. The percentage of cells assigned to specific clusters is shown for individual mice. Statistical significance was calculated by unpaired t test, p-value is shown in italics. Median is shown.

F-H. Cluster 4 was reanalyzed separately. **F.** UMAP projection showing two subclusters identified by unsupervised clustering. **G.** The intensity of the blue color indicates the level of expression of *Itgα4* or *Il7r* in individual cells. **H.** Projection of subclusters 0 and 1 on the original UMAP plot.

I. Ly5.1 OT-I T cells (5×10^4) were adoptively transferred into Treg-depleted DEREG$^+$ RIP.OVA mice or DEREG$^-$ RIP.OVA mice. The next day, mice were immunized with DC-OVA. On day 3 post-immunization, spleens were collected and analyzed by flow cytometry. The cells were gated into four subsets based on the expression of KLRK1 and CD49d (ITGA4) and the expression of IL-7R and CD103 in these subsets was compared. A representative experiment out of five in total is shown.

Figure 6

A. On day 0 and 1, DEREG$^+$ RIP.OVA mice were treated with DT in order to deplete Tregs, and DEREG$^-$ RIP.OVA mice were treated or not with IL-2/S4B6 on days 0, 1, and 2. On day 3, spleens were collected and analyzed by flow cytometry. Percentage of super-effectors (defined as KLRK1$^+$ CD49d$^-$) and double-positive KLRK1$^+$ CD49d$^+$ cells among CD8$^+$ T cells is shown. Untreated n=6, DT n=7, IL-2/S4B6 n=8.

B-F. OT-I *Rag2*$^{-/-}$ mice were treated with OVA peptide (single dose on day 0, n=7), and/or IL-2/S4B6 (3 doses, days 0, 1 and 2, n=7 mice per group) or left untreated (n=6). Spleens were collected and analyzed by flow cytometry on day 3. **B.** A representative experiment, showing percentages of naïve, antigen-experienced KLRK1$^-$ CD49d$^+$ (AE), double-positive KLRK1$^+$ CD49d$^+$ (DP) effector, and KLRK1$^+$ CD49d$^-$

super-effector (SE) cells among OT-I T cells. **C.** Number of KLRK1$^+$ CD49d$^-$ super-effector (SE) cells. **D.** GZMB levels in OT-I T cells. Left: A representative histogram. Right: Geometric mean fluorescence intensity (MFI) of anti-GZMB-eFluor 660 antibody on OT-I T cells. Obtained values were normalized to the average of MFI of untreated samples in each experiment (=1). **E.** IL-7R expression in KLRK1$^+$ CD49d$^-$ cells (SE gate). Left: Representative histogram. Level of IL-7R expression on naïve OT-I cells is shown in grey and serves as a positive control. Right: Number of IL-7R$^+$ SE cells. **F.** IL-7R expression in CD49d$^+$ KLRK1$^-$ antigen-experienced (AE), CD49d$^+$ KLRK1$^+$ double-positive (DP), CD49d$^-$ KLRK1$^+$ super effector (SE), and CD49d$^-$ KLRK1$^-$ naïve OT-I T cells from mice treated with OVA + IL-2/S4B6. Left: A representative histogram. Right: Percentage of IL-7R$^+$ cells among OT-I T cells in indicated populations.

G. OT-I *Rag2*$^{-/-}$ mice were treated with OVA peptide (day 0), and/or IL-2/S4B6 (days 0, 1 and 2) or left untreated. Spleens were collected on day 3. KLRK1$^+$ CD8$^+$ or KLRK1$^-$ CD8$^+$ cells were sorted and adoptively transferred into recipient RIP.OVA mice, which have received a mixture of target OVA-pulsed CTV-loaded and unpulsed CFSE-loaded splenocytes from Ly5.1 mice at ~1:1 ratio earlier the same day. The next day, the spleens were analyzed for the presence of Ly5.1 donor cells by flow cytometry. Ratio of unpulsed (CFSE$^+$) to OVA pulsed (CTV$^+$) target cells was determined and normalized to control recipients which did not receive OT-I T cells (=1). KLRK1$^-$ (no treatment) n=6, KLRK1$^-$ (OVA + IL-2/JES6) n=11, KLRK1$^+$ (OVA + IL-2/JES6) n=13, KLRK1$^+$ (OVA peptide) n=6. Four independent experiments.

H-K. Human CD8$^+$ T cells atlas was generated by integrating 14 scRNAseq data sets from blood of healthy donors. The gene expression data after the removal of MAIT cells were projected into a 2D UMAP plot. **H.** The assignment of individual cells to clusters identified by unsupervised clustering. Individual clusters were matched to established CD8$^+$ T cell subsets based on the expression of their signature markers (see Fig. S6H). **I.** The intensity of the blue color indicates the level of expression of indicated genes in individual cells. **J.** The percentage of CD8$^+$ T cells assigned to the super-effector-like CD8$^+$ T-cell cluster in individual donors (n=14). **K.** Left: Clonally expanded T cells were identified based on their TCRαβ VDJ sequences. The intensity of the red color indicates the size of individual clones. Right: T cells with recovered complete TCRαβ VDJ information are shown in green.

Statistical significance was calculated by Kruskal-Wallis test (p-value is shown in italics) with Dunn's post-test (* <0.05, **<0.01, ***<0.001). Median is shown.

Figure 7

A-C. On day 0, BALB/C mice were inoculated with BCL1 leukemia cells. On days 11 and 24 post inoculation, mice received doxorubicin (Dox), with or without anti-CD4 or anti-CD8 depletion mAbs. On three consecutive days, mice were treated with IL-2/JES6. n=16 mice per group in two independent

experiments with the exception of "Dox + IL-2/JES6 + αCD8" conditions where three mice in the second experiment did not tolerate anti-CD8 administration for unknown reasons and were removed. **A.** Scheme of the experiment. **B.** Survival curves. **C.** The detection of the BCL1 IgM/IgD in the serum on day 54 by ELISA using an anti-idiotypic antibody. Percentage of mice with undetectable BCL1, detectable BCL1, and dead mice in each group is shown.

D-E. On day 0, C57Bl/6J mice were inoculated with B16F10 melanoma cells. On day 6, mice received doxorubicin (Dox). On three consecutive days, mice were treated with IL-2/JES6. n=16 mice per group in two independent experiments. **D**. Scheme of the experiment showing also the eventual treatment with anti-CD4 or anti-CD8 depletion mAb relevant for Figure S7B. **E**. Survival curves.

Statistical significance was calculated by Log-rank (Mantel-Cox) test (survival) or Fisher's exact test (ELISA, two groups of the outcome: mice with undetectable BCL1 vs. mice with detectable BCL1 or dead). P-value is shown in italics. Median is shown.

References

1. Josefowicz, S.Z. and A. Rudensky, *Control of Regulatory T Cell Lineage Commitment and Maintenance.* Immunity, 2009. **30**(5): p. 616-625.
2. Bennett, C.L., et al., *The immune dysregulation, polyendocrinopathy, enteropathy, X-linked syndrome (IPEX) is caused by mutations of FOXP3.* Nature Genetics, 2001. **27**(1): p. 20-21.
3. Brunkow, M.E., et al., *Disruption of a new forkhead/winged-helix protein, scurfin, results in the fatal lymphoproliferative disorder of the scurfy mouse.* Nature Genetics, 2001. **27**(1): p. 68-73.
4. Wildin, R.S., et al., *X-linked neonatal diabetes mellitus, enteropathy and endocrinopathy syndrome is the human equivalent of mouse scurfy.* Nature Genetics, 2001. **27**(1): p. 18-20.
5. Chinen, T., et al., *An essential role for the IL-2 receptor in T-reg cell function.* Nature Immunology, 2016. **17**(11): p. 1322-1333.
6. Laidlaw, B.J., et al., *Production of IL-10 by CD4(+) regulatory T cells during the resolution of infection promotes the maturation of memory CD8(+) T cells.* Nature Immunology, 2015. **16**(8): p. 871-+.
7. Kalia, V., et al., *Quiescence of Memory CD8(+) T Cells Is Mediated by Regulatory T Cells through Inhibitory Receptor CTLA-4.* Immunity, 2015. **42**(6): p. 1116-1129.
8. McNally, A., et al., *CD4+CD25+ regulatory T cells control CD8+ T-cell effector differentiation by modulating IL-2 homeostasis.* Proc Natl Acad Sci U S A, 2011. **108**(18): p. 7529-34.
9. Kastenmuller, W., et al., *Regulatory T cells selectively control CD8+ T cell effector pool size via IL-2 restriction.* J Immunol, 2011. **187**(6): p. 3186-97.
10. Pace, L., et al., *Regulatory T Cells Increase the Avidity of Primary CD8(+) T Cell Responses and Promote Memory.* Science, 2012. **338**(6106): p. 532-536.
11. Schildknecht, A., et al., *FoxP3+ regulatory T cells essentially contribute to peripheral CD8+ T-cell tolerance induced by steady-state dendritic cells.* Proc Natl Acad Sci U S A, 2010. **107**(1): p. 199-203.
12. Green, E.A., et al., *CD4(+)CD25(+) T regulatory cells control anti-islet CD8(+) T cells through TGF-beta-TGF-beta receptor interactions in type 1 diabetes.* Proceedings of the National Academy of Sciences of the United States of America, 2003. **100**(19): p. 10878-10883.
13. King, C.G., et al., *T cell affinity regulates asymmetric division, effector cell differentiation, and tissue pathology.* Immunity, 2012. **37**(4): p. 709-20.
14. Kurts, C., et al., *Major histocompatibility complex class I-restricted cross-presentation is biased towards high dose antigens and those released during cellular destruction.* Journal of Experimental Medicine, 1998. **188**(2): p. 409-414.
15. Lahl, K., et al., *Selective depletion of Foxp3(+) regulatory T cells induces a scurfy-like disease.* Journal of Experimental Medicine, 2007. **204**(1): p. 57-63.
16. Kim, J.M., J.P. Rasmussen, and A.Y. Rudensky, *Regulatory T cells prevent catastrophic autoimmunity throughout the lifespan of mice.* Nature Immunology, 2007. **8**(2): p. 191-197.
17. Stepanek, O., et al., *Coreceptor scanning by the T cell receptor provides a mechanism for T cell tolerance.* Cell, 2014. **159**(2): p. 333-45.
18. Polhill, T., et al., *IL-2/IL-2Ab complexes induce regulatory T cell expansion and protect against proteinuric CKD.* J Am Soc Nephrol, 2012. **23**(8): p. 1303-8.
19. Liu, R., et al., *Expansion of regulatory T cells via IL-2/anti-IL-2 mAb complexes suppresses experimental myasthenia.* Eur J Immunol, 2010. **40**(6): p. 1577-89.
20. Boyman, O., et al., *Selective stimulation of T cell subsets with antibody-cytokine immune complexes.* Science, 2006. **311**(5769): p. 1924-1927.

21. Spangler, J.B., et al., *Antibodies to Interleukin-2 Elicit Selective T Cell Subset Potentiation through Distinct Conformational Mechanisms.* Immunity, 2015. **42**(5): p. 815-825.
22. Kim, R. and T. Kin, *Current and Future Therapies for Immunogenic Cell Death and Related Molecules to Potentially Cure Primary Breast Cancer.* Cancers (Basel), 2021. **13**(19).
23. Bosch, A.J.T., et al., *A minimum number of autoimmune T cells to induce autoimmunity?* Cell Immunol, 2017. **316**: p. 21-31.
24. Tomala, J. and M. Kovar, *IL-2/anti-IL-2 mAb immunocomplexes: A renascence of IL-2 in cancer immunotherapy?* Oncoimmunology, 2016. **5**(3): p. e1102829.
25. Marchingo, J.M., et al., *Antigen affinity, costimulation, and cytokine inputs sum linearly to amplify T cell expansion.* Science, 2014. **346**(6213): p. 1123-1127.
26. Akkaya, B., et al., *Regulatory T cells perform antigen specific suppression by depleting cognate peptide-MHC class II via trogocytosis.* Journal of Immunology, 2019. **202**(1).
27. Prajapati, K., et al., *Functions of NKG2D in CD8(+) T cells: an opportunity for immunotherapy.* Cell Mol Immunol, 2018. **15**(5): p. 470-479.
28. Lee, S.J., et al., *CD134 Costimulation Couples the CD137 Pathway to Induce Production of Supereffector CD8 T Cells That Become IL-7 Dependent.* J Immunol, 2007. **179**(4): p. 2203-14.
29. Barsoumian, H.B., E.S. Yolcu, and H. Shirwan, *4-1BB Signaling in Conventional T Cells Drives IL-2 Production That Overcomes CD4+CD25+FoxP3+ T Regulatory Cell Suppression.* PLoS One, 2016. **11**(4): p. e0153088.
30. Oh, H.S., et al., *4-1BB Signaling Enhances Primary and Secondary Population Expansion of CD8+ T Cells by Maximizing Autocrine IL-2/IL-2 Receptor Signaling.* PLoS One, 2015. **10**(5): p. e0126765.
31. Palmer, E., A. Drobek, and O. Stepanek, *Opposing effects of actin signaling and LFA-1 on establishing the affinity threshold for inducing effector T-cell responses in mice.* Eur J Immunol, 2016. **46**(8): p. 1887-901.
32. Barnden, M.J., et al., *Defective TCR expression in transgenic mice constructed using cDNA-based alpha- and beta-chain genes under the control of heterologous regulatory elements.* Immunol Cell Biol, 1998. **76**(1): p. 34-40.
33. Jang, Y., et al., *Cutting Edge: Check Your Mice-A Point Mutation in the Ncr1 Locus Identified in CD45.1 Congenic Mice with Consequences in Mouse Susceptibility to Infection.* J Immunol, 2018. **200**(6): p. 1982-1987.
34. Kralova, J., et al., *Expression of Fluorescent Fusion Proteins in Murine Bone Marrow-derived Dendritic Cells and Macrophages.* J Vis Exp, 2018(140).
35. Kim, M.V., et al., *Murine in vivo CD8(+) T Cell Killing Assay.* Bio Protoc, 2014. **4**(13).
36. Slavin, S. and S. Strober, *Spontaneous Murine B-Cell Leukemia.* Nature, 1978. **272**(5654): p. 624-626.
37. Howe, K.L., et al., *Ensembl 2021.* Nucleic Acids Res, 2021. **49**(D1): p. D884-D891.
38. Zheng, G.X., et al., *Massively parallel digital transcriptional profiling of single cells.* Nat Commun, 2017. **8**: p. 14049.
39. Haberman, Y., et al., *Pediatric Crohn disease patients exhibit specific ileal transcriptome and microbiome signature.* J Clin Invest, 2014. **124**(8): p. 3617-33.
40. Andreatta, M., et al., *Interpretation of T cell states from single-cell transcriptomics data using reference atlases.* Nat Commun, 2021. **12**(1): p. 2965.
41. Kovanen, P.E., et al., *Global analysis of IL-2 target genes: identification of chromosomal clusters of expressed genes.* Int Immunol, 2005. **17**(8): p. 1009-21.
42. Lin, J.X., et al., *Critical Role of STAT5 transcription factor tetramerization for cytokine responses and normal immune function.* Immunity, 2012. **36**(4): p. 586-99.
43. Korotkevich, G., et al., *Fast gene set enrichment analysis.* bioRxiv, 2021: p. 060012.

44. Bais, A.S. and D. Kostka, *scds: computational annotation of doublets in single-cell RNA sequencing data.* Bioinformatics, 2020. **36**(4): p. 1150-1158.
45. Hahsler, M., M. Piekenbrock, and D. Doran, *dbscan: Fast Density-Based Clustering with R.* Journal of Statistical Software, 2019. **91**(1): p. 1-30.

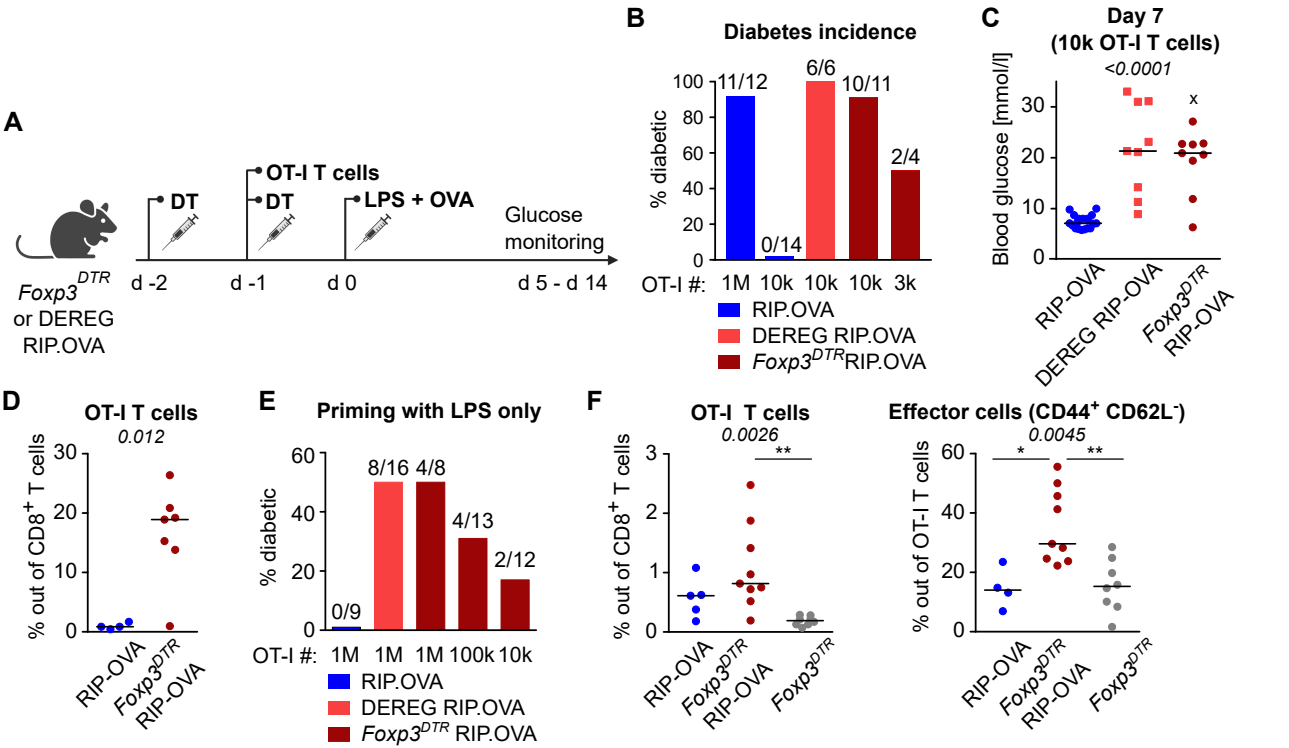
A
Foxp3DTR or DEREG RIP.OVA
DT
OT-I T cells
DT
LPS + OVA
Glucose monitoring
d -2
d -1
d 0
d 5 - d 14
B
Diabetes incidence
% diabetic
11/12
0/14
6/6
10/11
2/4
OT-I #: 1M 10k 10k 10k 3k
RIP.OVA
DEREG RIP.OVA
Foxp3DTRRIP.OVA
C
Day 7
(10k OT-I T cells)
<0.0001
Blood glucose [mmol/l]
RIP-OVA
DEREG RIP-OVA
Foxp3DTR RIP-OVA
D
OT-I T cells
0.012
% out of CD8+ T cells
RIP-OVA
Foxp3DTR RIP-OVA
E
Priming with LPS only
% diabetic
0/9
8/16
4/8
4/13
2/12
OT-I #: 1M 1M 1M 100k 10k
RIP.OVA
DEREG RIP.OVA
Foxp3DTR RIP.OVA
F
OT-I T cells
0.0026
% out of CD8+ T cells
Effector cells (CD44+ CD62L-)
0.0045
% out of OT-I T cells

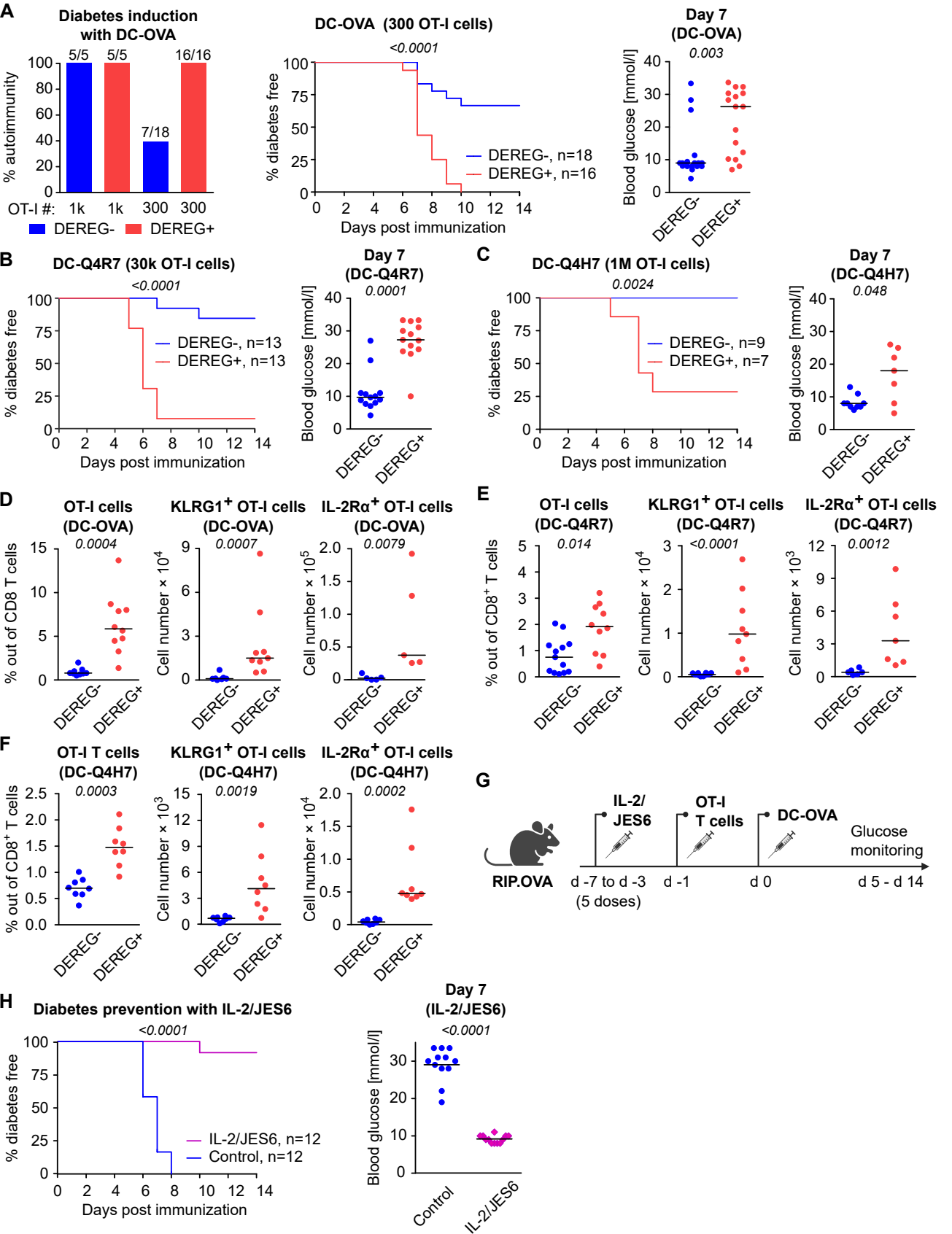
A
Diabetes induction with DC-OVA
% autoimmunity
5/5
5/5
7/18
16/16
OT-I #: 1k 1k 300 300
DEREG- DEREG+
DC-OVA (300 OT-I cells)
<0.0001
% diabetes free
DEREG-, n=18
DEREG+, n=16
Days post immunization
Day 7 (DC-OVA)
0.003
Blood glucose [mmol/l]
B
DC-Q4R7 (30k OT-I cells)
<0.0001
DEREG-, n=13
DEREG+, n=13
Day 7 (DC-Q4R7)
0.0001
C
DC-Q4H7 (1M OT-I cells)
0.0024
DEREG-, n=9
DEREG+, n=7
Day 7 (DC-Q4H7)
0.048
D
OT-I cells (DC-OVA)
0.0004
% out of CD8 T cells
KLRG1+ OT-I cells (DC-OVA)
0.0007
Cell number × 10^4
IL-2Rα+ OT-I cells (DC-OVA)
0.0079
Cell number × 10^5
E
OT-I cells (DC-Q4R7)
0.014
% out of CD8+ T cells
KLRG1+ OT-I cells (DC-Q4R7)
<0.0001
Cell number × 10^4
IL-2Rα+ OT-I cells (DC-Q4R7)
0.0012
Cell number × 10^3
F
OT-I T cells (DC-Q4H7)
0.0003
% out of CD8+ T cells
KLRG1+ OT-I cells (DC-Q4H7)
0.0019
Cell number × 10^3
IL-2Rα+ OT-I cells (DC-Q4H7)
0.0002
Cell number × 10^4
G
RIP.OVA
IL-2/ JES6
OT-I T cells
DC-OVA
Glucose monitoring
d -7 to d -3 (5 doses)
d -1
d 0
d 5 - d 14
H
Diabetes prevention with IL-2/JES6
<0.0001
IL-2/JES6, n=12
Control, n=12
Day 7 (IL-2/JES6)
<0.0001
Control
IL-2/JES6

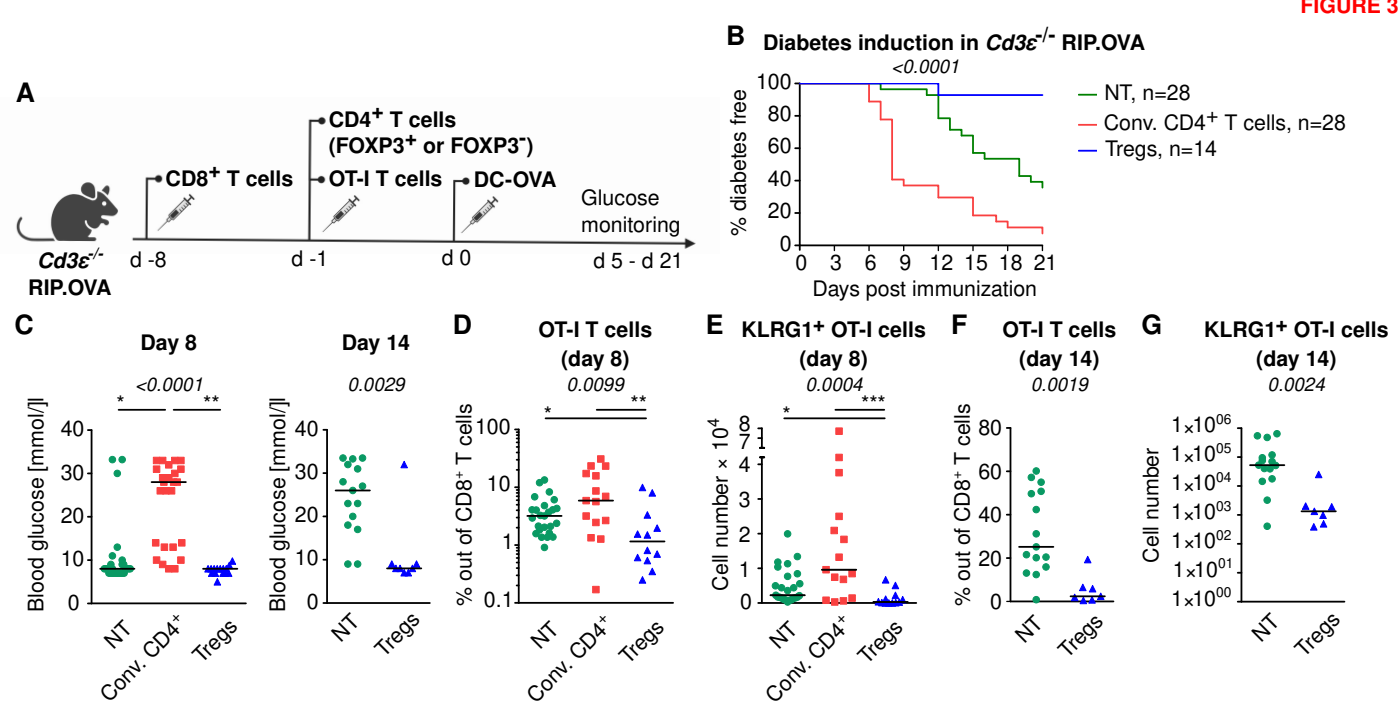
A
CD8+ T cells
CD4+ T cells
(FOXP3+ or FOXP3-)
OT-I T cells
DC-OVA
Glucose
monitoring
Cd3ε-/-
RIP.OVA
d -8
d -1
d 0
d 5 - d 21
B
Diabetes induction in Cd3ε-/- RIP.OVA
<0.0001
% diabetes free
Days post immunization
NT, n=28
Conv. CD4+ T cells, n=28
Tregs, n=14
C
Day 8
<0.0001
Blood glucose [mmol/l]
Day 14
0.0029
NT
Conv. CD4+
Tregs
D
OT-I T cells
(day 8)
0.0099
% out of CD8+ T cells
E
KLRG1+ OT-I cells
(day 8)
0.0004
Cell number × 10^4
F
OT-I T cells
(day 14)
0.0019
G
KLRG1+ OT-I cells
(day 14)
0.0024
Cell number

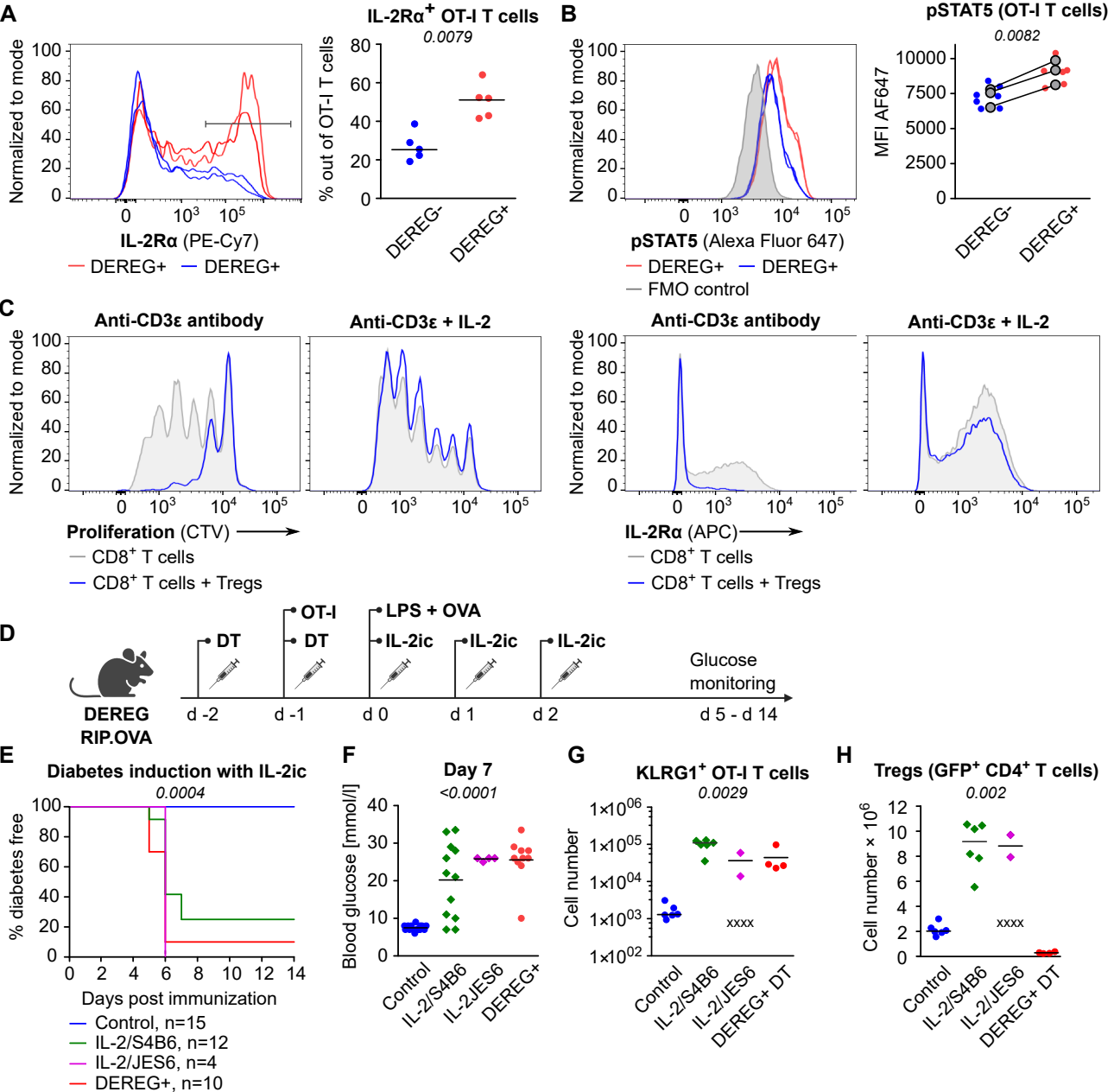
A
Normalized to mode
IL-2Rα (PE-Cy7)
DEREG+ DEREG+
IL-2Rα+ OT-I T cells
0.0079
% out of OT-I T cells
DEREG-
DEREG+
B
Normalized to mode
pSTAT5 (Alexa Fluor 647)
DEREG+ DEREG+
FMO control
pSTAT5 (OT-I T cells)
0.0082
MFI AF647
DEREG-
DEREG+
C
Anti-CD3ε antibody
Anti-CD3ε + IL-2
Normalized to mode
Proliferation (CTV)
CD8+ T cells
CD8+ T cells + Tregs
Anti-CD3ε antibody
Anti-CD3ε + IL-2
Normalized to mode
IL-2Rα (APC)
CD8+ T cells
CD8+ T cells + Tregs
D
DEREG
RIP.OVA
DT
OT-I
DT
LPS + OVA
IL-2ic
IL-2ic
IL-2ic
Glucose monitoring
d -2
d -1
d 0
d 1
d 2
d 5 - d 14
E
Diabetes induction with IL-2ic
0.0004
% diabetes free
Days post immunization
Control, n=15
IL-2/S4B6, n=12
IL-2/JES6, n=4
DEREG+, n=10
F
Day 7
<0.0001
Blood glucose [mmol/l]
Control
IL-2/S4B6
IL-2JES6
DEREG+
G
KLRG1+ OT-I T cells
0.0029
Cell number
xxxx
Control
IL-2/S4B6
IL-2/JES6
DEREG+ DT
H
Tregs (GFP+ CD4+ T cells)
0.002
Cell number × 10^6
xxxx
Control
IL-2/S4B6
IL-2/JES6
DEREG+ DT

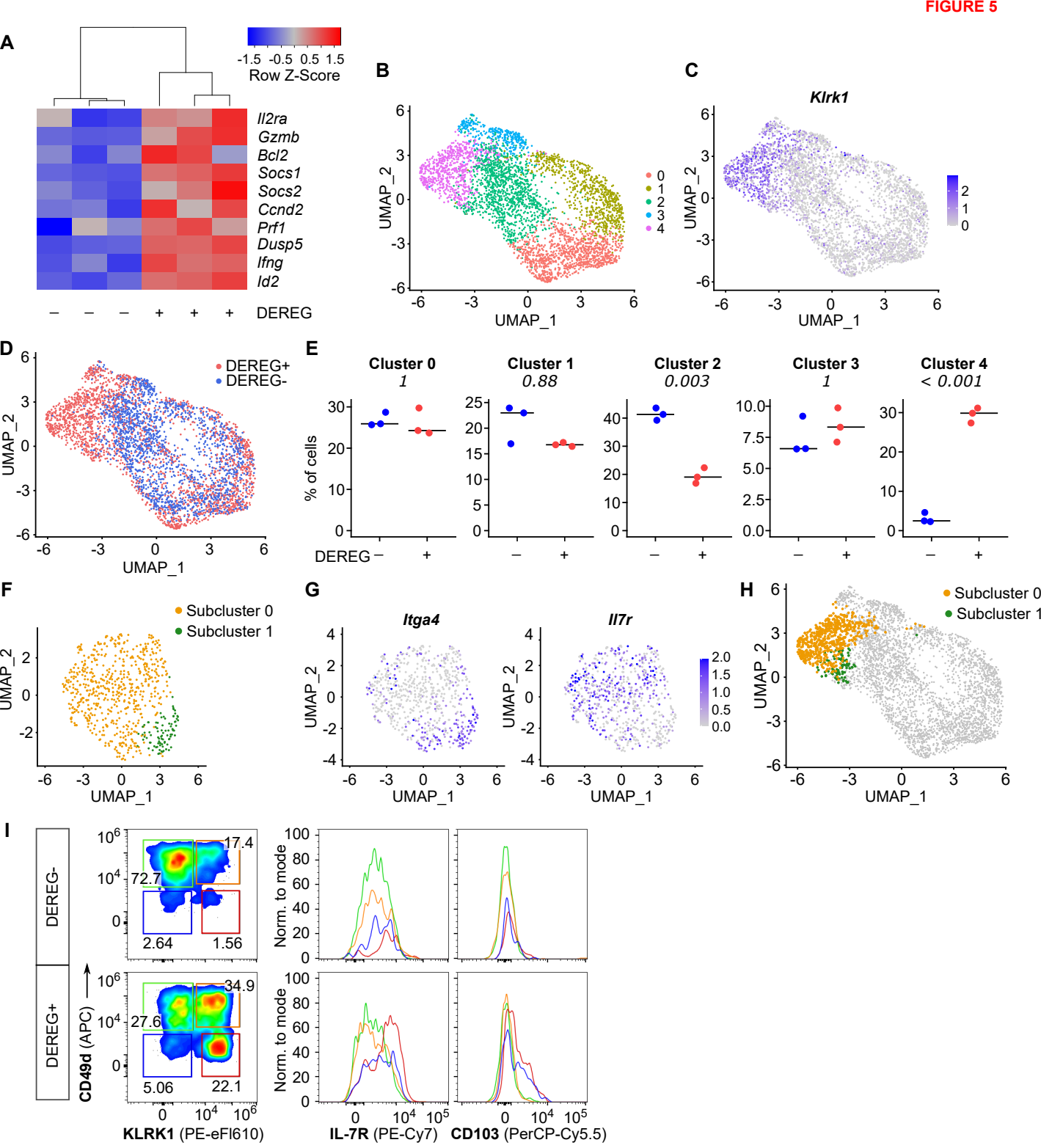
A
-1.5 -0.5 0.5 1.5
Row Z-Score
Il2ra
Gzmb
Bcl2
Socs1
Socs2
Ccnd2
Prf1
Dusp5
Ifng
Id2
– – – + + +
DEREG
B
UMAP_2
UMAP_1
0
1
2
3
4
C
Klrk1
UMAP_2
UMAP_1
2
1
0
D
DEREG+
DEREG-
UMAP_2
UMAP_1
E
Cluster 0
1
Cluster 1
0.88
Cluster 2
0.003
Cluster 3
1
Cluster 4
< 0.001
% of cells
DEREG – +
F
Subcluster 0
Subcluster 1
UMAP_2
UMAP_1
G
Itga4
Il7r
UMAP_2
UMAP_1
2.0
1.5
1.0
0.5
0.0
H
Subcluster 0
Subcluster 1
UMAP_2
UMAP_1
I
DEREG-
DEREG+
CD49d (APC)
17.4
72.7
2.64
1.56
34.9
27.6
5.06
22.1
KLRK1 (PE-eFl610)
Norm. to mode
IL-7R (PE-Cy7)
CD103 (PerCP-Cy5.5)

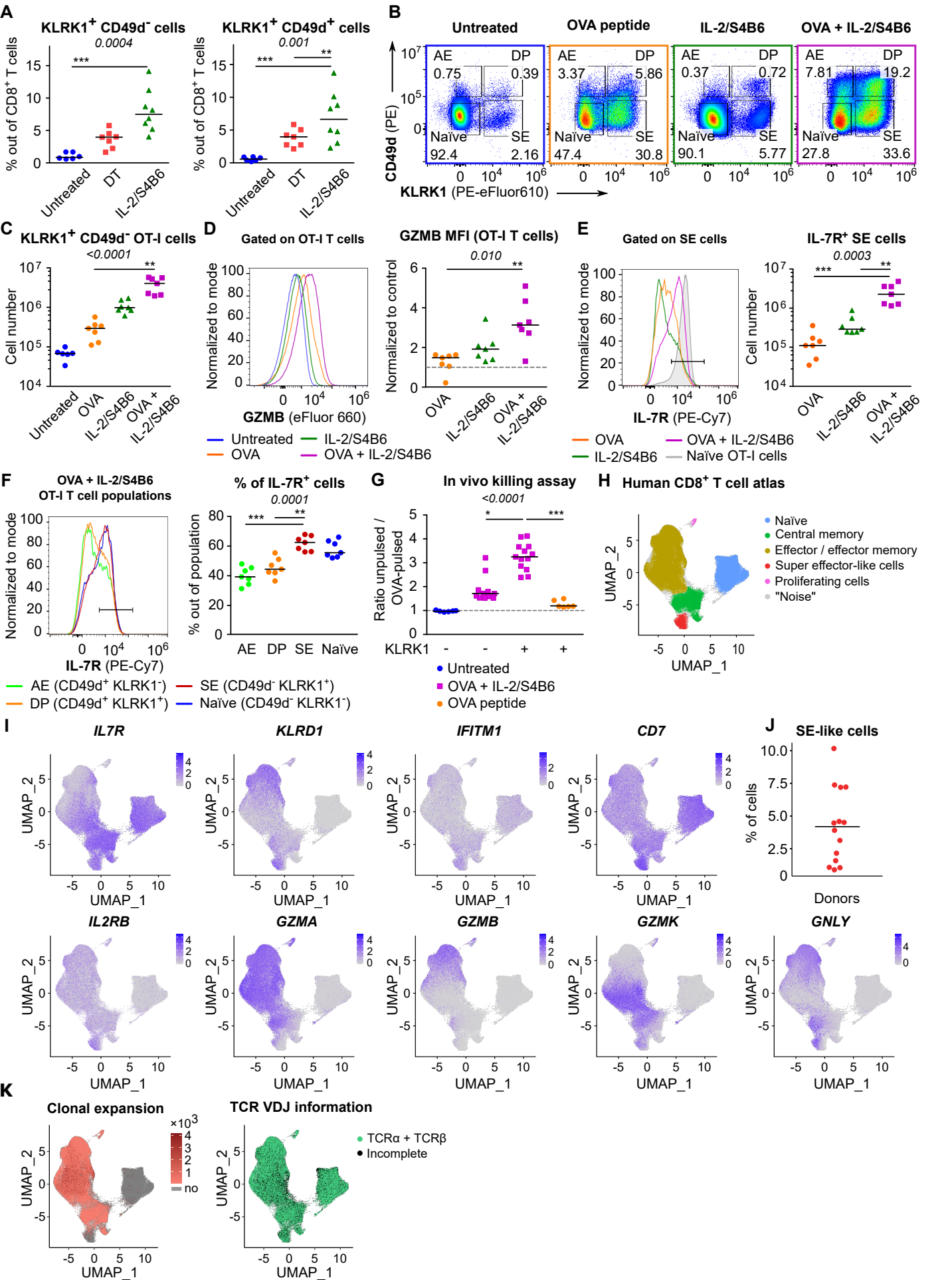
A
KLRK1+ CD49d- cells
0.0004
***
% out of CD8+ T cells
Untreated
DT
IL-2/S4B6
KLRK1+ CD49d+ cells
0.001
***
**
B
Untreated
OVA peptide
IL-2/S4B6
OVA + IL-2/S4B6
AE
DP
Naïve
SE
0.75
0.39
92.4
2.16
3.37
5.86
47.4
30.8
0.37
0.72
90.1
5.77
7.81
19.2
27.8
33.6
CD49d (PE)
KLRK1 (PE-eFluor610)
C
KLRK1+ CD49d- OT-I cells
<0.0001
**
Cell number
Untreated
OVA
IL-2/S4B6
OVA + IL-2/S4B6
D
Gated on OT-I T cells
Normalized to mode
GZMB (eFluor 660)
GZMB MFI (OT-I T cells)
0.010
**
Normalized to control
Untreated
OVA
IL-2/S4B6
OVA + IL-2/S4B6
E
Gated on SE cells
Normalized to mode
IL-7R (PE-Cy7)
IL-7R+ SE cells
0.0003
***
**
Cell number
OVA
IL-2/S4B6
OVA + IL-2/S4B6
Naïve OT-I cells
F
OVA + IL-2/S4B6
OT-I T cell populations
Normalized to mode
IL-7R (PE-Cy7)
% of IL-7R+ cells
0.0001
***
**
% out of population
AE
DP
SE
Naïve
AE (CD49d+ KLRK1-)
DP (CD49d+ KLRK1+)
SE (CD49d- KLRK1+)
Naïve (CD49d- KLRK1-)
G
In vivo killing assay
<0.0001
*
***
Ratio unpulsed / OVA-pulsed
KLRK1
Untreated
OVA + IL-2/S4B6
OVA peptide
H
Human CD8+ T cell atlas
UMAP_2
UMAP_1
Naïve
Central memory
Effector / effector memory
Super effector-like cells
Proliferating cells
"Noise"
I
IL7R
KLRD1
IFITM1
CD7
IL2RB
GZMA
GZMB
GZMK
GNLY
J
SE-like cells
% of cells
Donors
K
Clonal expansion
×10^3
no
TCR VDJ information
TCRα + TCRβ
Incomplete

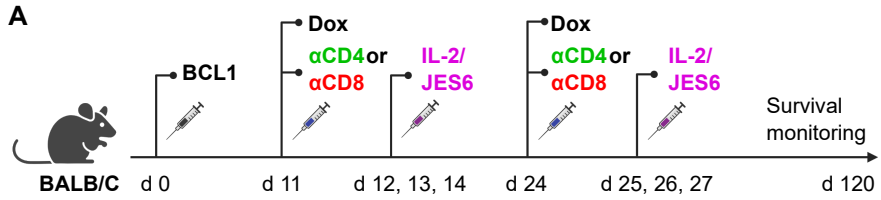
A
BCL1
Dox
αCD4 or
αCD8
IL-2/
JES6
Dox
αCD4 or
αCD8
IL-2/
JES6
Survival
monitoring
BALB/C
d 0
d 11
d 12, 13, 14
d 24
d 25, 26, 27
d 120

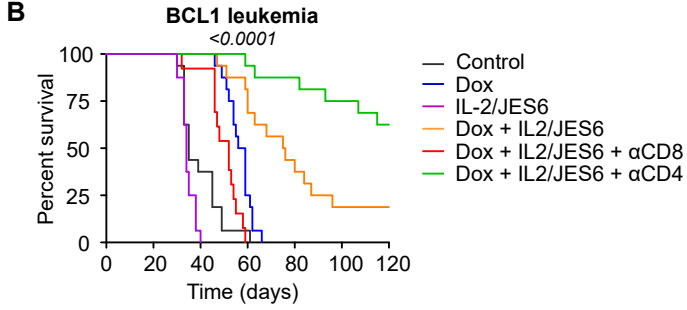
B
BCL1 leukemia
<0.0001
Percent survival
100
75
50
25
0
0
20
40
60
80
100
120
Time (days)
Control
Dox
IL-2/JES6
Dox + IL2/JES6
Dox + IL2/JES6 + αCD8
Dox + IL2/JES6 + αCD4

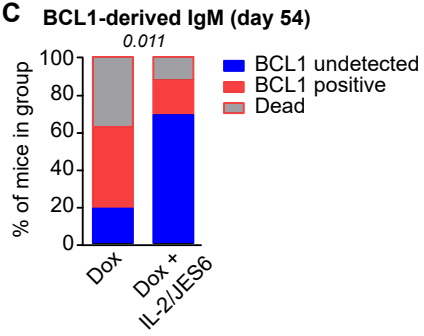
C
BCL1-derived IgM (day 54)
0.011
% of mice in group
100
80
60
40
20
0
Dox
Dox +
IL-2/JES6
BCL1 undetected
BCL1 positive
Dead

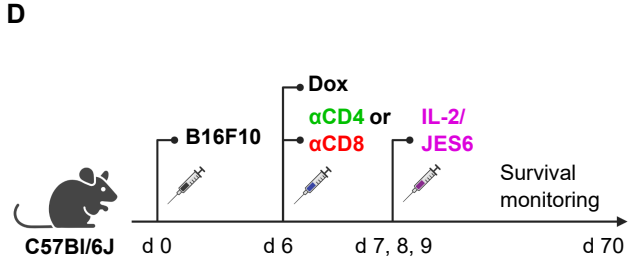
D
Dox
B16F10
αCD4 or
αCD8
IL-2/
JES6
Survival
monitoring
C57Bl/6J
d 0
d 6
d 7, 8, 9
d 70

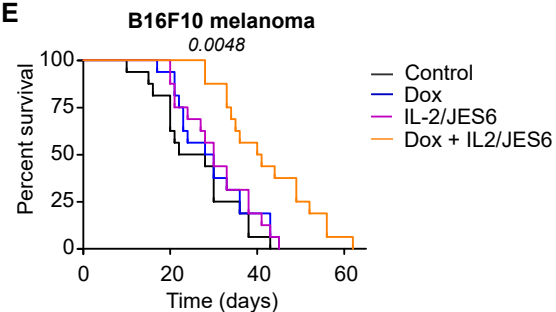
E
B16F10 melanoma
0.0048
Percent survival
100
75
50
25
0
0
20
40
60
Time (days)
Control
Dox
IL-2/JES6
Dox + IL2/JES6

Figure S1

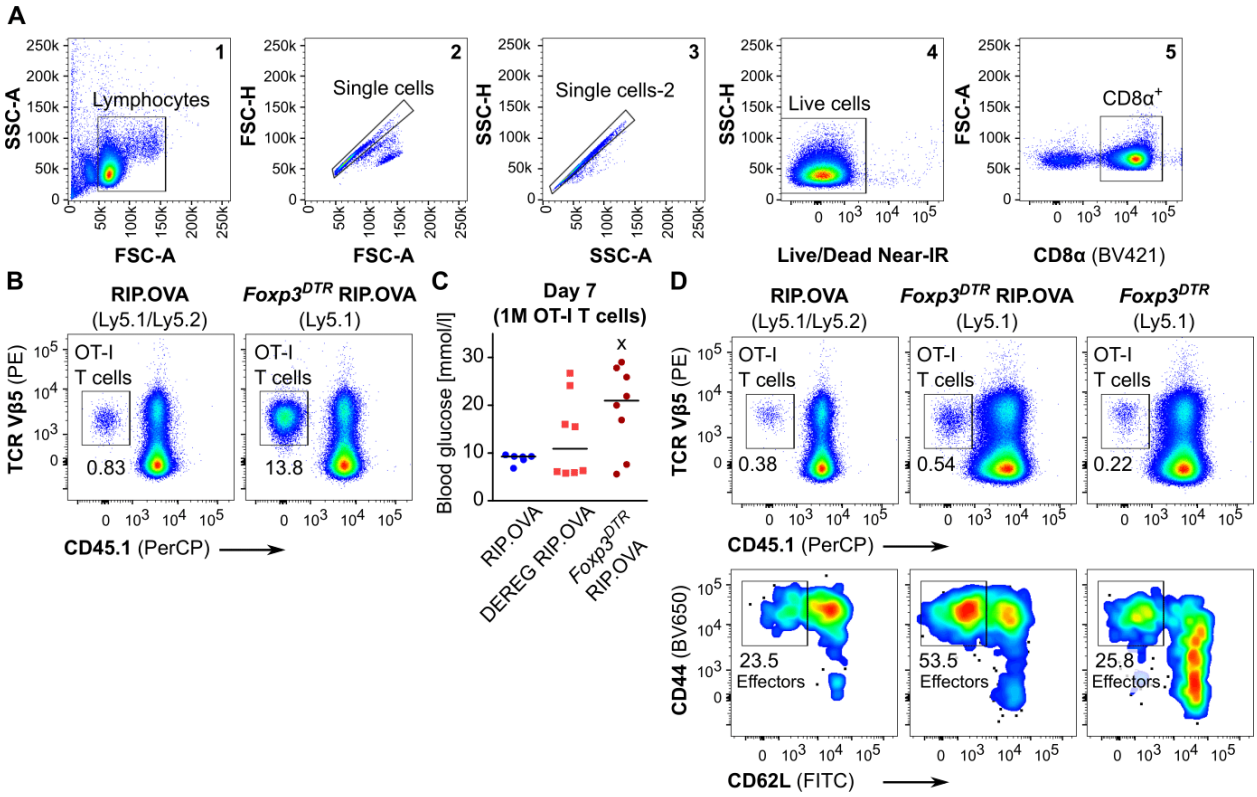

A. Gating strategy for the experiment shown in Fig. 1D. $CD4^+$ T cells and B cells were depleted via magnetic bead separation prior to the analysis. **B.** Representative dot plots for the experiment shown in Fig. 1D. **C.** Blood glucose concentration (day 7) in the experiment shown in Fig. 1E (10^6 transferred OT-I T cells). RIP.OVA n=6, DEREG RIP.OVA n=8, *Foxp3*^{DTR} RIP.OVA n=8. One *Foxp3*^{DTR} RIP.OVA mouse died before the measurement (shown as "x"). Median is shown. **D.** Representative dot plots for the experiment shown in Fig. 1F.

Figure S2

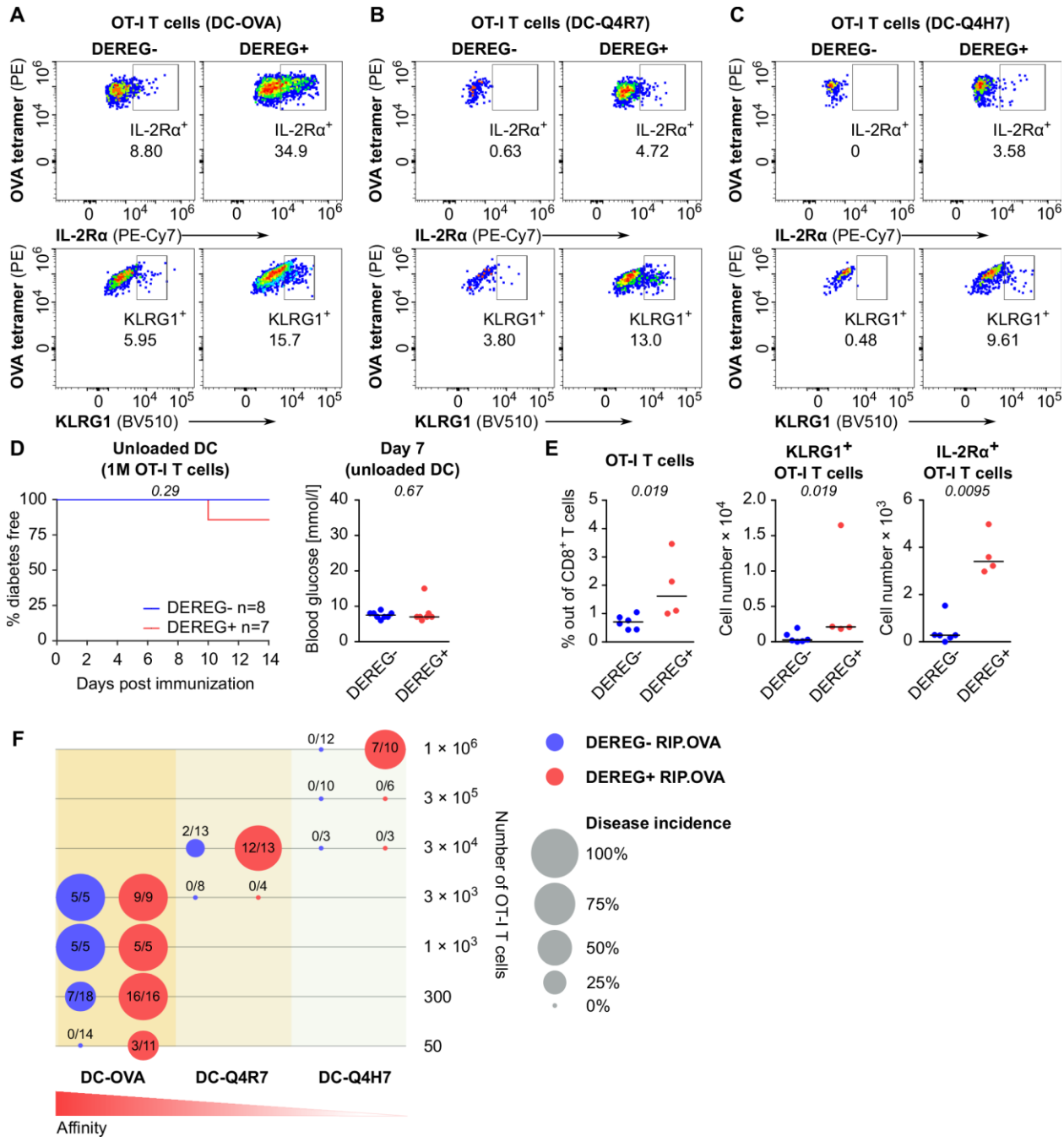

A. Representative dot plots for the experiment shown in Fig. 2D. **B.** Representative dot plots for the experiment shown in Fig. 2E. **C.** Representative dot plots for the experiment shown in Fig. 2F. **D-E.** Treg-depleted DEREG^{+} RIP.OVA mice and control DEREG^{-} RIP.OVA mice received 10^{6} OT-I T cells. The next day, they were immunized with unloaded DC. **D.** Urine glucose level was monitored on a daily basis. Left: Survival curve. Number of mice per group is indicated. Right: Blood glucose concentration on day 7 post-

immunization. **E.** On day 6 post-immunization, spleens were collected and analyzed by flow cytometry. Percentage of OT-I T cells among $CD8^+$ T cells, count of $KLRG1^+$ OT-I T cells, and count of IL-$2R\alpha^+$ OT-I T cells are shown. $DEREG^-$ n=6, $DEREG^+$ n=4. **F.** Bubble chart illustrating diabetes incidence in $DEREG^+$ RIP.OVA and $DEREG^-$ RIP.OVA mice immunized with DC loaded with indicated peptides vs. numbers of transferred OT-I T cells. Number of diabetic mice and total number of mice per group is indicated.

Statistical significance was calculated by Log-rank (Mantel-Cox) test (survival) or two-tailed Mann-Whitney test (glucose concentration and flow cytometry analysis), p-value is shown in italics. Median is shown.

Figure S3

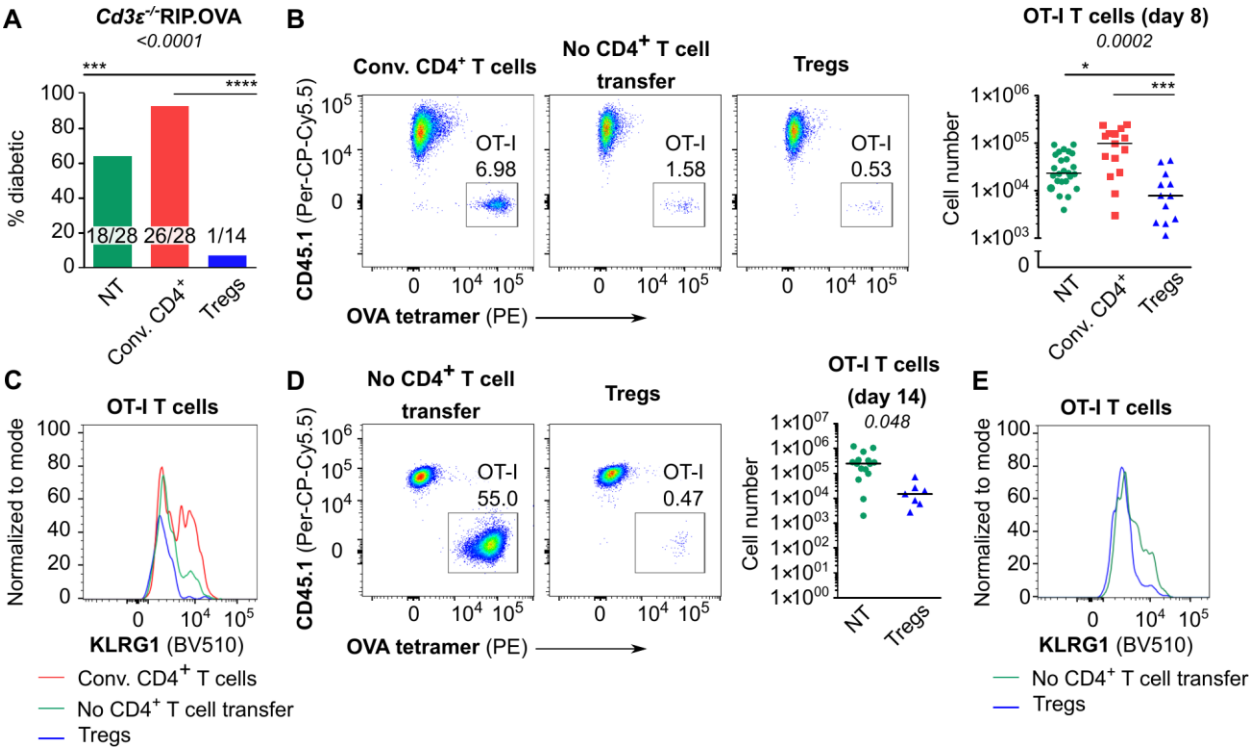

A. Percentage of diabetic mice in individual groups in the experiment shown in Fig. 3A. Number of diabetic mice and total number of mice per group is indicated.

B-C. In the experimental setup shown in Fig. 3A, spleens were collected on day 8 post-immunization and analyzed by flow cytometry. **B.** Left: Percentage of OT-I T cells among $CD8^+$ T cells. A representative experiment out of five in total. Right: Number of OT-I T cells is shown. NT n=25, Conv. $CD4^+$ n=15, Tregs n=12. **C.** KLRG1 expression on OT-I T cells on day 8, a representative histogram.

D-E. In the experimental setup shown in Fig. 3A, spleens were collected on day 14 post-immunization and analyzed by flow cytometry. **D.** Left: Percentage of OT-I T cells among $CD8^+$ T cells. Representative plots are shown. Right: Number of OT-I T cells is shown. NT n=15, Tregs n=7. **E.** KLRG1 expression on OT-I T cells on day 14. A representative experiment out of 3 in total.

Statistical significance was calculated using Chi-square test (p-value is shown in italics) and Fisher's exact post-test (***<0.001, ****<0.0001) for comparison of two groups of the outcomes: diabetic mice vs. diabetes-free mice (A). Statistical significance for flow cytometry analysis was calculated by Kruskal-Wallis test (p-value is shown in italics) with Dunn's post-test (* <0.05, ***<0.001, ****<0.0001) for comparison of three groups (B), or two-tailed Mann-Whitney test for comparison of two groups (D). Median is shown.

Figure S4

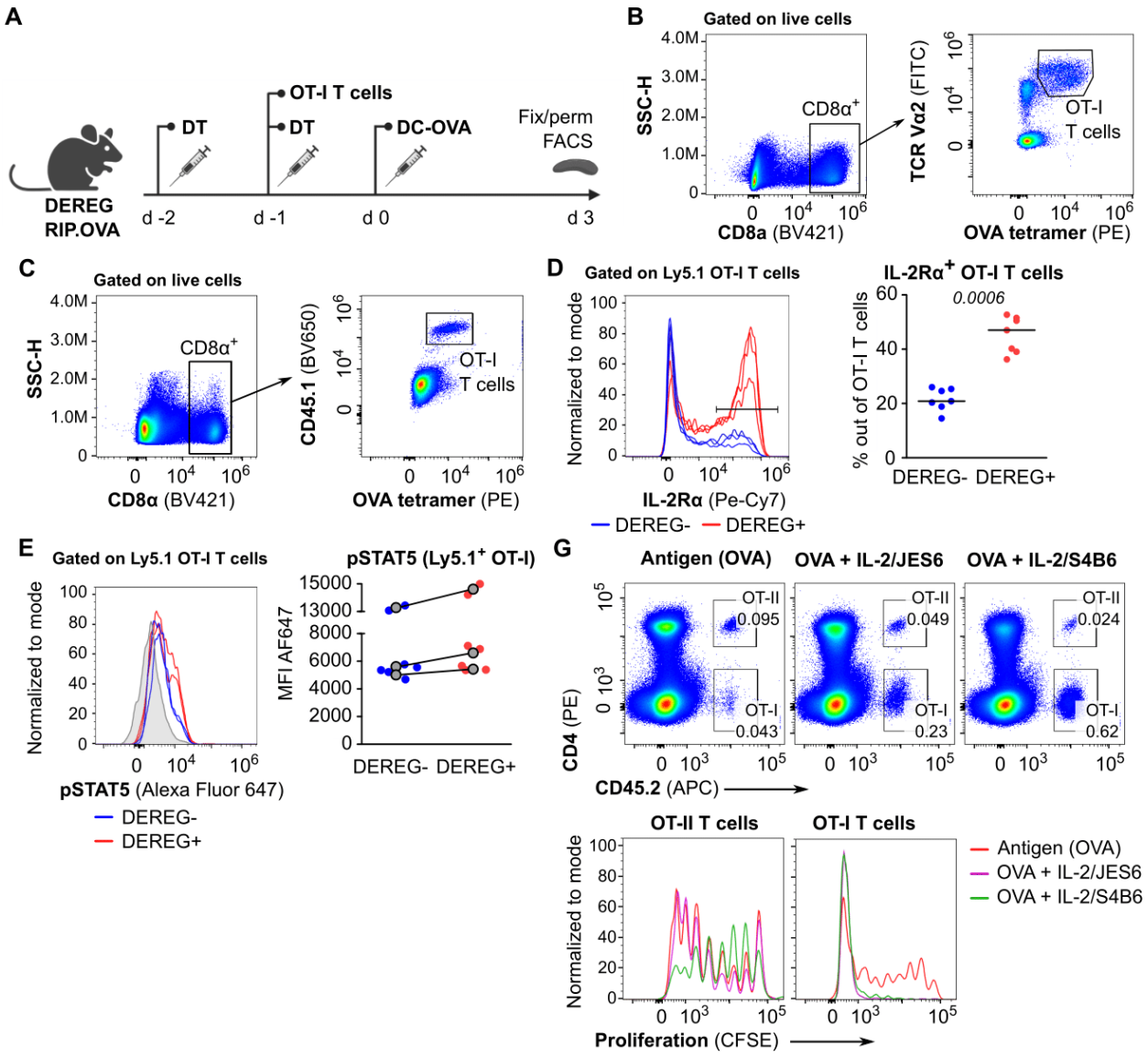

A. Scheme of the experiments described in Fig. 4A-C and Fig. S4B-E. **B.** Gating strategy for the experiment shown in Fig. 4A. **C-E.** The experiment described in Fig. 4A was modified by using congenic Ly5.1 OT-I T cells for the adoptive transfer. **C.** The gating strategy. **D.** IL-2Rα expression on OT-I Ly5.1 T cells. Left: a representative experiment out of 3 in total. Right: Percentage of IL-2Rα$^+$ cells among OT-I Ly5.1 T cells, n=7 mice per group. **E.** pSTAT5 expression in OT-I Ly5.1 T cells. Left: a representative experiment out of 3 in total. Right: Geometric mean fluorescence intensity (MFI) of anti-pSTAT5-Alexa Fluor 647 on Ly5.1 OT-I T cells. Mean of MFI values for each genotype per experiment are shown as a grey dots. Lines connect data from corresponding experiments. n=7 mice per group.

G. OT-I $CD8^+$ and OT-II $CD4^+$ T cells (both Ly5.2) were labeled with CFSE and adoptively transferred into Ly5.1 mice as a mixture (0.75×10^6 $CD8^+$ OT-I + 1.5×10^6 $CD4^+$ OT-II T cells), followed by the administration of OVA protein with or without IL-2ic (IL-2/S4B6 or IL-2/JES6). On day 5 post-immunization, spleens were collected and analyzed by flow cytometry. Top: Representative staining showing $CD45.2^+$ OT-I ($CD4^-$) and OT-II ($CD4^+$) T cells among viable cells. Bottom: Proliferation is indicated by the CFSE dilution. Representative histograms for OT-I and OT-II T cells.

Statistical significance was calculated by two-tailed Mann-Whitney test, p-value is shown in italics. Median is shown.

Figure S5

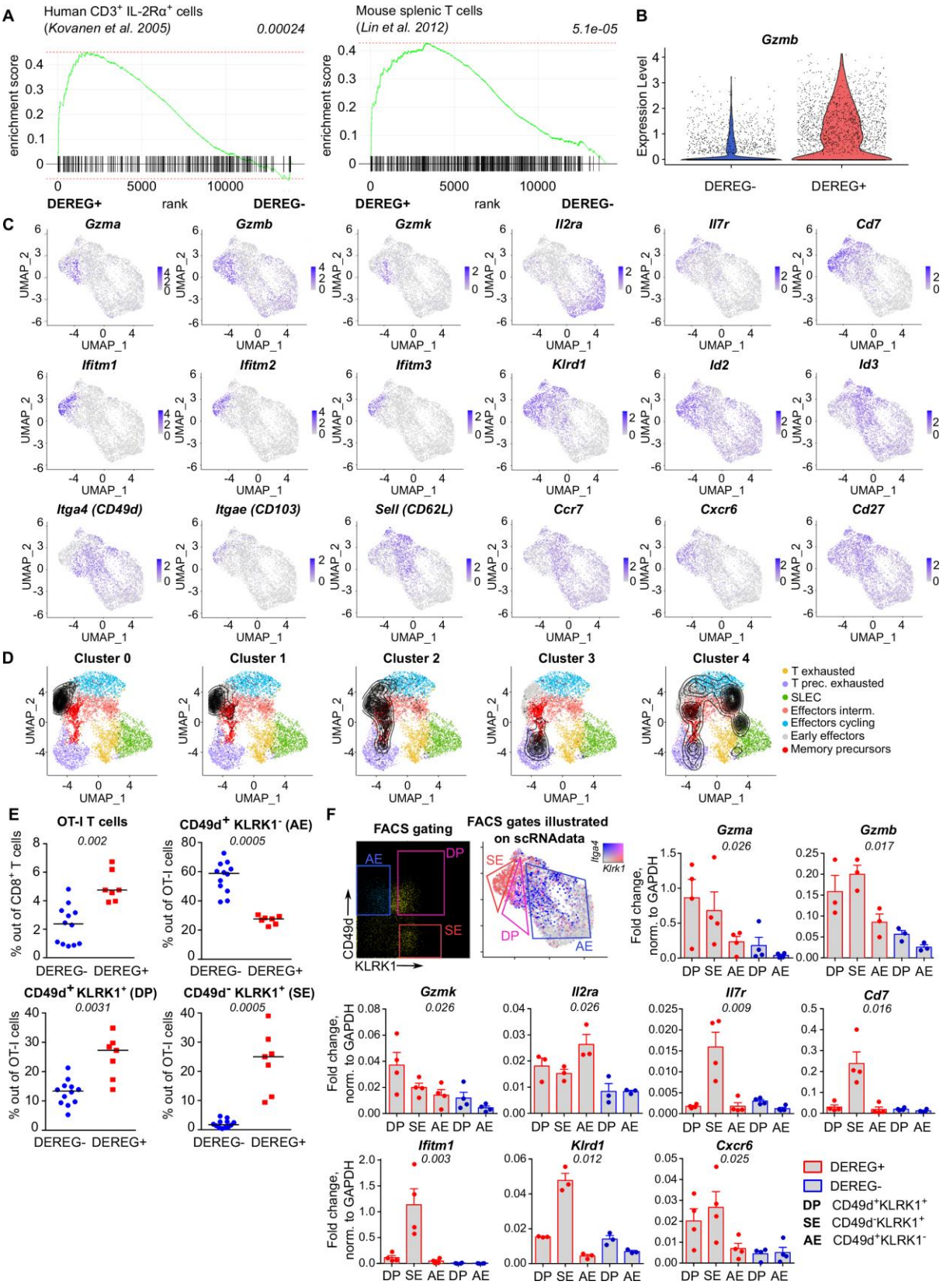

A-D. Additional analysis for the scRNAseq experiment shown in Fig. 5A-H. **A.** Gene set enrichment analyses comparing the ranked expression of IL-2 induced genes in DEREG$^+$ versus DEREG$^-$ samples. The list of IL-2-responsive genes is based on the indicated publications [40, 41]. P-value (shown in italics) is estimated based on an adaptive multi-level split Monte-Carlo scheme. **B.** Violin plot indicating the expression of *Gzmb* in OT-I T cells primed in DEREG$^-$ and DEREG$^+$ mice. **C.** The intensity of the blue color indicates the level of expression of indicated genes in individual cells. **D.** Projection of clusters of primed OT-I T cells (Fig. 5B) on the UMAP visualization of CD8$^+$ T cells subsets formed during an anti-viral response using TILPRED algorithm.

E. Aggregate results of the experiments described in Fig. 4I. The percentages of OT-I T cells among CD8$^+$ T cells, and percentages of CD49d$^+$ KLRK1$^-$ antigen-experienced (AE), CD49d$^+$ KLRK1$^+$ double-positive (DP) effector, and CD49d$^-$ KLRK1$^+$ super-effector (SE) cells among OT-I T cells are shown. DEREG$^-$ n=12, DEREG$^+$ n=7. Median is shown. Statistical significance was calculated using two-tailed Mann-Whitney test, p-value is shown in italics.

F. Ly5.1 OT-I T cells (5×10^4) were transferred into Treg-depleted DEREG$^+$ RIP.OVA mice and DEREG$^-$ RIP.OVA mice. The next day, mice were immunized with DC-OVA. On day 3 post immunization, splenic CD49d$^+$ KLRK1$^-$ antigen-experienced (AE), CD49d$^+$ KLRK1$^+$ double-positive (DP), and CD49d$^-$ KLRK1$^+$ super effector (SE) OT-I T cells (identified as Ly5.1$^+$ CD8$^+$) were FACS-sorted as indicated and analyzed via RT-qPCR. The correspondence of the FACS gates to scRNAseq clusters is shown. The expression of indicated genes was normalized to *Gapdh*. Mean + SEM is indicated. Four independent experiments. Statistical significance was calculated by Kruskal-Wallis test, p-value is shown in italics.

Figure S6

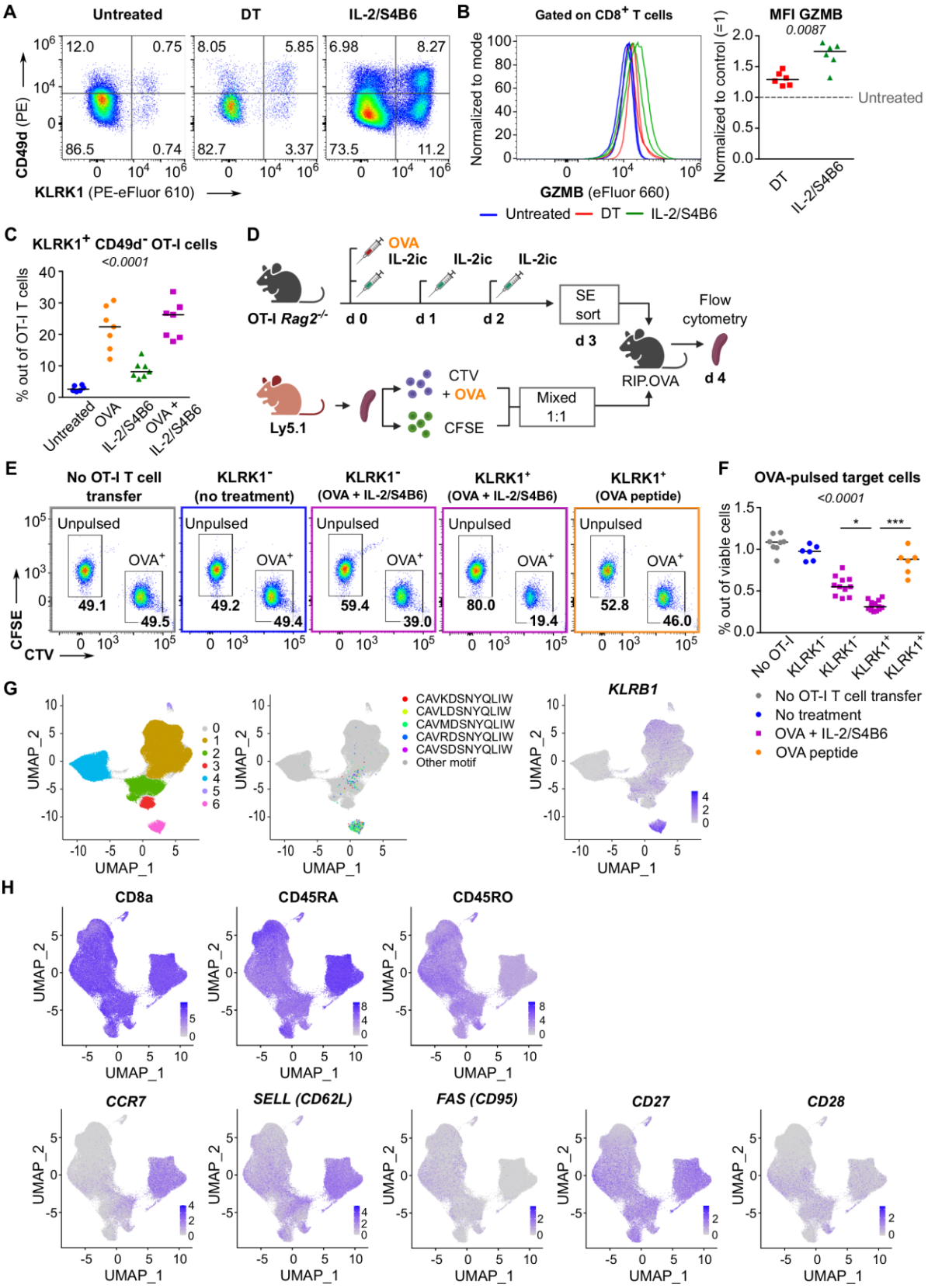

A. Representative dot plots for the experiment shown in Fig. 6A.

B. GZMB levels in $CD8^+$ T cells from the experiment shown in Fig. 6A. Left: A representative histogram. Right: Geometric mean fluorescence intensity (MFI) of anti-GZMB-eFluor 660 antibody on $CD8^+$ T cells was determined. Obtained values were normalized to the average of MFI of untreated samples in each experiment (=1). Six mice per group.

C. Quantification of super-effector $KLRK1^+$ $CD49d^-$ T cells in the experiment showed in Fig. 6B (untreated n=6, OVA n=7, IL-2/S4B6 n=7, OVA+IL-2/S4B6 n=7).

D-F. Additional analyses of the experiment shown in Fig. 6G. **D.** Scheme of the experiment. **E.** A representative experiment out of 4 in total. **F.** The percentage of OVA-pulsed target cells out of all viable splenocytes. No OT-I T cell transfer n=8, $KLRK1^-$ (no treatment) n=6, $KLRK1^-$ (OVA + IL-2/JES6) n=11, $KLRK1^+$ (OVA + IL-2/JES6) n=13, $KLRK1^+$ (OVA peptide) n=6.

G. Identification of MAIT cells in the Human $CD8^+$ T cell atlas. Left: UMAP projection. Individual cells are assigned to individual clusters based on unsupervised clustering. Cluster 6 corresponds to MAIT cells. Middle: Cells expressing five most abundant semi-invariant MAIT cell-specific receptor-alpha (TCRα) are shown. Right: The intensity of the blue color indicates the level of *KLRB1* expression (a MAIT cell marker) in individual cells.

H. The intensity of the blue color indicates the expression level of selected genes based on the detection using hash-tagged antibodies (top) or transcripts (bottom) in Human $CD8^+$ T cell atlas after the removal of MAIT cells.

Statistical significance was calculated by Kruskal-Wallis test (p-value is shown in italics) with Dunn's multiple comparison post-test (* <0.05, ***<0.001) (C, F), or two-tailed Mann-Whitney test (B). Median is shown.

Figure S7

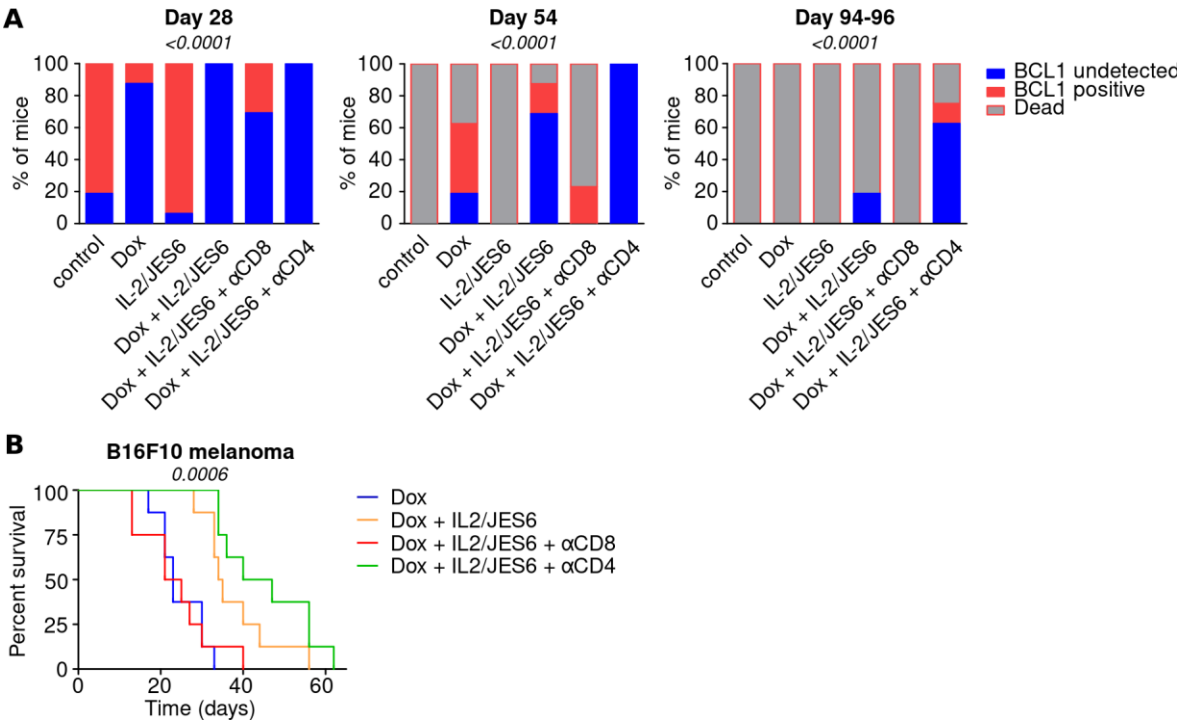

A. In experiments described in Fig. 7A-C, BCL1 IgM/IgD in the serum on days 28, 54, and 94-96 post tumor inoculation was detected by ELISA. n=16 mice per group in two independent experiments with two exceptions: (i) "Dox + IL-2/JES6 + αCD4" conditions on day 54 where the analysis failed for the second experiment and thus, n=8 mice and (ii) control conditions on day 54, when one mouse was not analyzed for technical reasons and thus, n=15. The data shown here include data shown in Fig. 7C. The statistical significance was calculated using Chi-square test (two groups of the outcomes: mice with undetectable BCL1 vs. mice with detectable BCL1 or dead).

B. On day 0, C57Bl/6J mice were inoculated with B16F10 melanoma cells. On day 6, mice received doxorubicin (Dox) with/without anti-CD4 or anti-CD8 depletion mAb. On three consecutive days, mice were treated with IL-2/JES6 (see Fig. 7D). Survival curves. n=8 mice per group in one experiments. The data shown here partially overlap with data shown in Fig. 7E. There were two experiments in total, but only the second experiment had the mouse groups with the depletion of $CD8^+$ or $CD4^+$ cells. Fig. 7E shows pooled data for all conditions included in both experiments. Here, results from the second experiment are shown. Statistical significance was calculated by Log-rank (Mantel-Cox) test.

Table S1

Differentially expressed genes for all clusters shown in Figure 5B. The used differential expression criteria were fold change above 2, minimum of 0.1 difference in the fraction of detection between each cluster and the rest of the cells and adjusted p-value below 0.01. For each gene, the fractions of cells with at least one detected transcript in the tested cluster (pct.1) or among all other cells (pct.2) are listed. The columns 'p_val', 'avg_log2FC' and 'p_val_adj' show p-values (Mann Whitney U Test), log2 fold changes and adjusted p-values (Bonferroni correction).

Table S2

Differentially expressed genes between the super-effector-like cell cluster and all the remaining cells in the human $CD8^+$ atlas (after MAIT removal). The used differential expression criteria were average fold change above 1.5 and adjusted p-value below 0.01. For each gene, the fractions of super-effector-like cells (pct.1) or remaining cells (pct.2) with at least one detected transcript are listed. The columns 'p_val ', 'avg_log2FC' and 'p_val_adj' show p-values (Mann Whitney U Test), log2 fold changes and adjusted p-values (Bonferroni correction).